Cardiac Imaging in Patients With Ventricular Tachycardia

ABSTRACT: Ventricular tachycardia (VT) is a major cause of sudden cardiac death. The majority of malignant VTs occur in patients with structural heart disease. Multimodality imaging techniques play an integral role in determining the underlying etiology and prognostic significance of VT. In recent years, advances in imaging technology have enabled characterization of the structural arrhythmogenic substrate in patients with VT with increasing precision. In parallel with these advances, the role of cardiac imaging has expanded from a largely diagnostic tool to an adjunctive tool to guide interventional approaches for treatment of VT. Invasive and noninvasive imaging techniques, often used in combination, have made it possible to integrate structural and electrophysiological information during VT ablation procedures. An important area of current development is the use of noninvasive imaging techniques based on body surface electrocardiographic mapping to elucidate the mechanisms of VT. In the future, these techniques may provide a priori information on mechanisms of VT in patients undergoing interventional procedures. This review provides an overview of the role of cardiac imaging in patients with VT.

Saagar Mahida, MD, PhD
Frédéric Sacher, MD, PhD
Rémi Dubois, PhD
Maxime Sermesant, PhD
Frank Bogun, MD
Michel Haïssaguerre, MD
Pierre Jaïs, MD
Hubert Cochet, MD, PhD

Ventricular tachycardia (VT) is a major cause of sudden cardiac death. The vast majority of VTs occur in patients with structural cardiac abnormalities because of reentry within myocardial scar. Implantable cardiac defibrillators (ICDs) are indicated in patients with VT who are deemed to have a high risk of sudden cardiac death. A subset of patients with ICDs experience recurrent shocks, which are associated with significant morbidity. VT ablation has emerged as an effective adjunctive technique to reduce the burden of ICD shocks.[1]

Cardiac imaging plays an integral role in determining the underlying etiology and prognostic significance of VT. Over the past 2 decades, cardiac imaging in patients with VT has evolved from the use of predominantly echocardiographic techniques to define ventricular structure and function, to the use of multimodality imaging techniques such as cardiac magnetic resonance imaging (CMR), multidetector cardiac computed tomography (MDCT), and nuclear imaging to characterize the structural VT substrate with a high degree of precision.

In parallel with advances in imaging technology, the role of cardiac imaging has expanded from a largely diagnostic tool to an adjunctive tool to guide VT ablation procedures. Integrating information on the structural VT substrate, as defined by noninvasive imaging, and the electrophysiological substrate, as defined by invasive electroanatomic mapping (EAM), has the potential to enhance safety and efficacy of ablation procedures. Additionally, imaging techniques are

Correspondence to: Saagar Mahida, MD, PhD, Department of Cardiac Electrophysiology, Liverpool Heart and Chest Hospital, Liverpool, UK L14 3PE. E-mail saagar.mahida@lhch.nhs.uk

Key Words: cardiac imaging ■ ventricular tachycardia

emerging as valuable tools to assess efficacy of lesion formation after VT ablation.

An important area of current development is the use of noninvasive imaging techniques that define activation patterns of VT wavefronts to complement imaging of the structural arrhythmogenic substrate. The emergence of technologies such as body surface mapping is of particular interest in this context. The following review will focus on the role of cardiac imaging in patients with VT.

IMAGING AS A DIAGNOSTIC TOOL

Accurate characterization of the underlying etiology of VT using cardiac imaging has an important impact on therapeutic decisions, including ICD implantation and VT ablation. According to recent guidelines, transthoracic echocardiography (TTE) and coronary angiography remain first-line diagnostic imaging modalities in patients presenting with VT, whereas CMR is recommended when TTE does not provide accurate assessment of ventricular function or evaluation of structural changes.[2] TTE represents a readily available and inexpensive tool for the assessment of cardiac structure, valve function, and quantification of the left ventricular ejection fraction. Echocardiographic analysis of wall thinning and echo density could potentially also identify regions of myocardial scar. However, the image resolution of TTE is not sufficient for detailed scar analysis. Furthermore, TTE is limited by suboptimal image quality in 10% to 15% of cases.[3]

Diagnostic Role of CMR

CMR provides excellent soft tissue image resolution and is widely regarded as the gold standard for imaging of the structural VT substrate. In addition to detailed assessment of cardiac morphology and function, CMR visualizes myocardial scar with a high degree of precision. The most widely used technique for CMR scar evaluation is based on measurement of the signal intensity of late gadolinium enhancement (LGE). A number of different signal intensity–based algorithms are currently used to define scar, including SD-based and maximum signal intensity–based algorithms.[4] It is important to note that although these techniques are effective for scar identification, there remains a lack of consensus regarding the optimal approach for scar quantification.[4]

Although LGE-CMR accurately identifies focal scar, its reliance on relative contrast between scarred and remote areas makes it less effective for identification of diffuse myocardial fibrosis.[5] To enhance the diagnostic performance of CMR in this context, myocardial T1 and extracellular volume mapping techniques are increasingly integrated into imaging protocols. T1 mapping identifies areas with increased interstitial space based on absolute values of longitudinal relaxation before and after loading the tissue with contrast media. Regions with increased interstitial space could be representative of fibrosis or inflammation. Extracellular volume mapping is derived from native and contrast-enhanced T1 maps and allows for the quantification of myocardial extracellular space and potentially acute myocardial inflammation.[5,6] T2 mapping, which is based on absolute values of transverse relaxation, also provides incremental information on the presence of myocardial edema and inflammation.[6]

CMR-based characterization of scar distribution and extent of scar transmurality provide important information to distinguish between ischemic cardiomyopathies (ICMs) and nonischemic cardiomyopathies (NICMs) (Figure 1A–1C). Further, the ability to detect subtle structural abnormalities, myocardial scar patterns, and myocardial inflammation allows differentiation between specific nonischemic etiologies such as myocarditis, sarcoid, and amyloid cardiomyopathies. Accurate measurement of myocardial thickness and characterization of fibrosis on CMR also provide incremental information for the diagnosis of hypertrophic cardiomyopathy.[7] In addition to scar definition, CMR is particularly effective for the assessment of right ventricular regional wall motion and quantification of ventricular volume and systolic function. Therefore, CMR plays an important role in the diagnosis of arrhythmogenic right ventricular cardiomyopathy.[8]

The value of CMR in the diagnostic workup of patients presenting with VT is underscored by studies demonstrating that CMR alters the underlying diagnoses in up to 50% of patients after an initial conventional diagnostic workup involving TTE and coronary angiography.[9] Furthermore, relevant myocardial disease is identified in up to 25% of patients categorized as having normal hearts based on non-CMR imaging.[9] Overall, these findings suggest that more widespread use of CMR may be desirable in patients presenting with VT, including among patients in whom the quality of echocardiographic imaging is sufficient.

Despite the superior image resolution afforded by CMR, the technique is associated with potential limitations in patients with device implants, which is of particular relevance in patients with VT. Concerns regarding the safety of CMR in patients with ICDs have been raised based on reports of local tissue heating, arrhythmia induction, and device software and hardware malfunction.[10] More recently, however, CMR in patients with conventional ICDs has been reported to be safe, with only isolated cases of software malfunction.[11] The emergence of magnetic resonance imaging (MRI)-compatible devices is predicted to largely overcome concerns relating to both software and hardware malfunction.[12] An additional limitation in patients with ICDs is device-related artifacts, which have the poten-

Circulation. 2017;136:2491–2507. DOI: 10.1161/CIRCULATIONAHA.117.029349

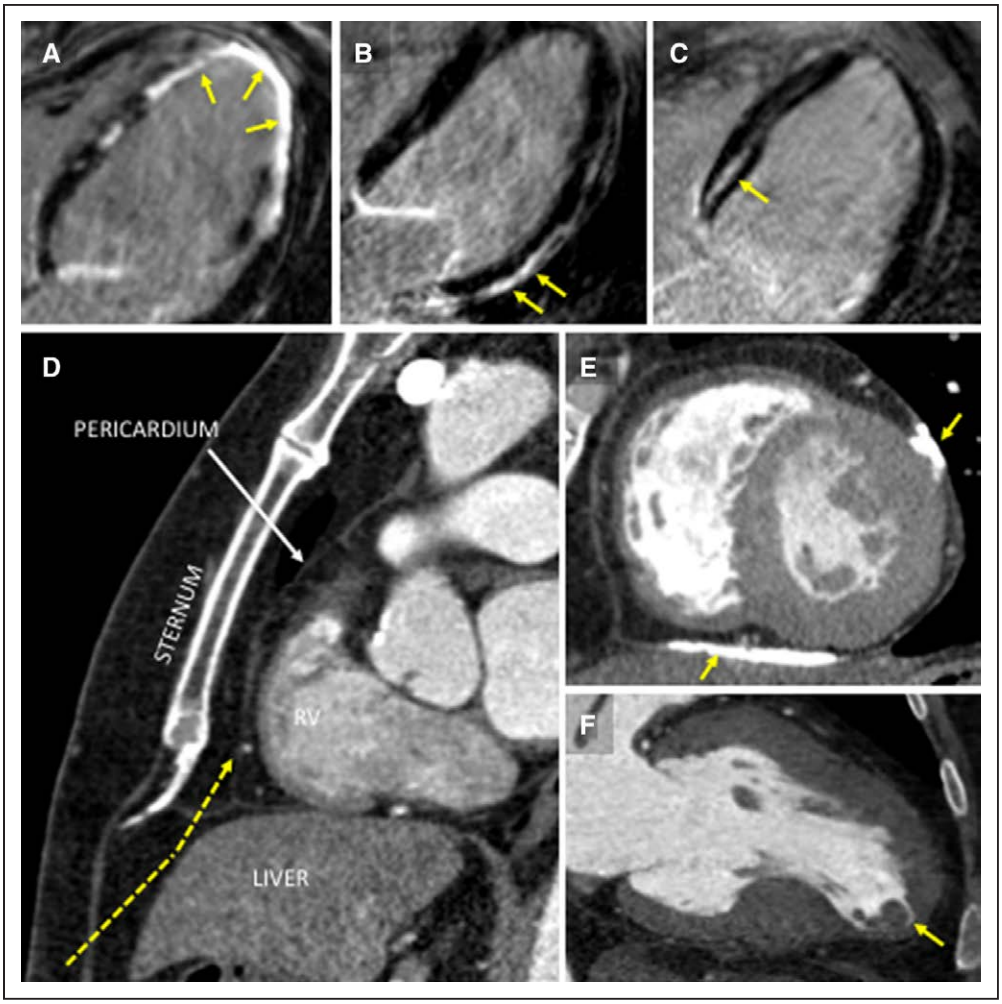

Figure 1. CMR imaging for defining VT substrate and determining optimal access for VT ablation.
Late gadolinium-enhanced CMR can assess the transmural distribution of VT substrate to devise the optimal access route. Scar distribution is predominantly subendocardial in ischemic scars (**A**), subepicardial in postinflammatory scars (**B**), or midwall in dilated cardiomyopathy (**C**). In the case of planning for epicardial access, CT can assess the anatomy of the subxyphoid access route (dashed yellow arrow in **D**) as well as the presence of pericardial calcification (**E**), which might limit catheter navigability within the pericardial space. Intracardiac thrombus at risk of emboli during endocardial mapping can be detected with transthoracic echocardiography, CMR, or CT (**F**). CMR indicates cardiac magnetic resonance; CT, computed tomography; and VT, ventricular tachycardia.

tial to significantly reduce the diagnostic yield of CMR. Scar imaging with LGE-CMR is particularly susceptible to ICD-related artifacts, with >50% of the ventricular segments affected by artifact.[13] Although modifications in imaging techniques, such as the use of wideband MRI, have been associated with superior scar characterization, artifact remains a major factor limiting the utility of MRI in patients with ICDs.

Diagnostic Role of Nuclear Imaging

Nuclear imaging techniques also potentially provide incremental diagnostic information in patients with VT. These techniques utilize radiolabel tracers conjugated to metabolically active molecules to identify regions with inducible myocardial ischemia (single-photon emission CT [SPECT] with thallium 201 [^{201}Tl-SPECT], ^{99m}Tc-sestamibi [^{99m}Tc-MIBI-SPECT], and ^{99m}Tc-tetrofosmin [^{99m}Tc-TF-SPECT], and positron-emission tomography [PET] scanning with ^{11}C-acetate, ^{13}N-ammonia, ^{15}O-water, and ^{82}Rb) and regions with active inflammation (^{18}fluorodeoxyglucose [^{18}F-FDG-PET]), and to distinguish between regions of scar and viable tissue (^{201}Tl-SPECT, ^{99m}Tc-MIBI-SPECT, ^{99m}Tc-TF-SPECT, and ^{18}F-FDG-PET).[14] Nuclear imaging techniques are commonly used to detect silent ischemia in patients presenting with VT. FDG-PET is also effective for distinguishing NICM etiologies related to myocardial inflammation.[15] The potential value of FDG-PET in patients with VT is highlighted by recent evidence demonstrating that in up to 50% of patients with ventricular arrhythmias and unexplained cardiomyopathies, the technique identifies an inflammatory etiology.[15] Overall, however, apart from specific cardiomyopathies such as sarcoid, nuclear medicine techniques have largely been superseded by CMR for imaging of the arrhythmogenic VT substrate.

Diagnostic Role of MDCT

The role of MDCT as a diagnostic tool in patients presenting with VT is relatively limited. Compared with CMR, a major advantage of MDCT is a significantly higher spatial resolution. Specifically, the spatial resolution of LGE CMR images is usually limited to 1.5 to 2 mm in plane, with ≤6- to 8-mm slice thickness. Although recent free-breathing methods enable CMR imaging at a near-isotropic spatial resolution of 1 to 2 mm^3, this remains largely below that which can be achieved with CT technology (close to 0.5 mm^3 on most systems).

Therefore, MDCT lends itself to noninvasive assessment of the coronary arteries, particularly in patients with low to intermediate probability of coronary artery disease.[16] In circumstances where CMR and TTE imaging is unavailable or suboptimal, MDCT may also be considered as an alternative modality for detailed assessment of myocardial structure and function.[2] As discussed in subsequent sections, MDCT can also be used for detailed characterization of scar.[17–19] However, MDCT is associated with a lower contrast-to-noise ratio within myocardial tissue, which contributes to inferior scar characterization relative to LGE-CMR. MDCT-based scar imaging, and indeed structural imaging, are currently largely limited to an adjunctive role during VT ablation procedures.

IMAGING AS A RISK STRATIFICATION TOOL

The presence of structural cardiac abnormalities is a major determinant of prognosis in patients presenting with VT. ICD implantation is recommended in patients with sustained VT, which is hemodynamically compromising and/or occurs in the context of structural heart disease.[20] It is important to note, however, that a dichotomous approach to risk stratification, based on the presence or absence of structural heart disease, is associated with important limitations. In recent years, significant interest has focused on developing more individualized risk stratification strategies based on advanced multimodality imaging. The importance of accurate risk stratification is not confined to appropriate selection of patients for ICD implantation. Identifying patients who are at particularly high risk of recurrent VT, and who may therefore benefit from early adjunctive antiarrhythmic drug therapy or VT ablation, is an important potential area of development.

The role of TTE for risk stratification is largely limited to making relatively subjective assessments of left ventricular ejection fraction and wall motion abnormalities. Based on its ability to precisely delineate myocardial scar, the role of LGE-CMR for more accurate risk stratification is an area of significant interest. The majority of studies on CMR-based risk stratification have focused on patients who have not previously experienced arrhythmic events. Although a detailed discussion on risk stratification in primary prevention populations is beyond the scope of this review, these studies have provided valuable insights into specific scar characteristics that may be associated with a higher arrhythmic risk.

As summarized in Table I in the online-only Data Supplement, the presence of scar has consistently been associated with increased arrhythmic risk in ICM and NICM, including hypertrophic cardiomyopathy, myocarditis, and sarcoidosis.[21–31] More specific scar characteristics, such as extent of scar, pattern of scar, size of the scar border zone, scar transmurality, scar heterogeneity, number of core islands, and the presence of conducting channels within scar, have also been implicated as modulators of risk in ICM and NICM cohorts.[21,22,32–47] However, these associations have not been consistent across studies.[37,43] Potential explanations for the lack of consistency include variation in techniques used to define scar and factors such as limited spatial resolution and partial volume averaging, which may reduce the accuracy of defining the extent of the scar border zone.[48]

The potential role of nuclear imaging techniques for risk stratification has been the subject of renewed interest. In addition to using FDG-PET and SPECT imaging for characterization of the structural VT substrate, imaging with compounds such as ^{11}C-meta-hydroxyephedrine (^{11}C-HED PET) and iodine-123-labeled-meta-iodobenzylguanidine (^{123}I-*m*IBG) allows assessment of sympathetic innervation, which is a potentially important risk modulator. As is the case in CMR-based risk stratification studies, nuclear imaging studies have mainly focused on primary prevention populations. Among ICM populations, the extent of scar as defined by SPECT scanning has been reported to predict ventricular arrhythmias.[49] Furthermore, studies involving a range of cardiomyopathies have reported that cardiac denervation and consequent inhomogeneity of innervation are associated with an increased risk of ventricular arrhythmia and sudden cardiac death.[50] It is important to note, however, that as is the case for LGE-CMR, the association between denervation and arrhythmic risk has not been consistent across studies.[51]

Overall, although advanced multimodality imaging techniques have emerged as potentially effective tools for risk stratification, lack of data from large randomized trials and inconsistent results from relatively small cohorts of patients have meant that these approaches have not been widely adopted into routine clinical practice.

IMAGING AS AN ADJUNCTIVE TOOL FOR VT ABLATION

The role of cardiac imaging in patients undergoing VT ablation is expanding. Specifically, imaging plays a potentially important role for preprocedural assessment of cardiac anatomy and myocardial scar, intraprocedural integration of the structural and electrophysiological VT substrate, and post procedural assessment of the efficacy of ablation. It important to note however, that despite promising results from early studies, there are currently no large clinical trials on efficacy of adjunctive imaging for VT ablation. Furthermore, the cost-effectiveness of these approaches remains to be proven.

Preprocedural Determination of the Optimal Access Route

A priori information on cardiac anatomy and 3-dimensional scar architecture has an important influence on planning the access route for VT ablation.[52] LGE-CMR accurately defines epicardial and intramural scar (Figure 1A–1C), the presence of which is an important determinant of VT ablation failure.[52] Among patients with epicardial substrates, success rates are enhanced by epicardial ablation. Epicardial access is, however, also associated with higher complication rates and is therefore not routinely performed as a first-line approach in patients undergoing VT ablation. Identification of the subset of patients who benefit from first-line epicardial ablation using LGE-CMR has been reported to significantly improve outcomes.[52] Along the same lines, the finding of intramural scar on CMR may justify the use of specific ablation techniques, such as needle and bipolar ablation, which potentially also enhance outcomes.[53]

Epicardial access for VT ablation involves a percutaneous subxiphoid approach into the pericardial space.[54] Imaging with MDCT or CMR can be used to assess the intricate anatomic relationship between the pericardium and surrounding structures to determine the needle trajectory that minimizes collateral damage to the diaphragm and intraabdominal organs. In addition, the finding of pericardial abnormalities, such as calcification or thickening on MDCT, or concordant patterns of regional displacement on tagged cine CMR, may suggest the presence of pericardial adhesions, which limit catheter navigability within the pericardial space.[55,56] The utility of cardiac imaging for preprocedural planning of the optimal access route is illustrated in Figure 1D and 1E.

Preprocedural Exclusion of Intracardiac Thrombus

Preprocedure imaging for left ventricular thrombi is important because of a potential risk of intraprocedural embolic complications during VT ablation. Although transthoracic echocardiography has traditionally been the predominant imaging modality for the detection of left ventricular thrombi, suboptimal image quality is a frequent limitation of the technique. In recent years, CMR and MDCT have emerged as superior imaging modalities for detailed assessment of left ventricular thrombi (Figure 1F).[57,58] Among patients with thrombi, the specific imaging characteristics of the thrombus have an important influence on the ablation strategy. Current guidelines suggest that, although left ventricular endocardial ablation can be performed in patients with a laminated thrombus, the presence of a mobile thrombus represents a contraindication.[59] Among selected patients with mobile thrombi, ablation with epicardial access only has been demonstrated to be a viable alternative ablation strategy.[60]

Intraprocedural Imaging for Guidance of VT Ablation

Current VT ablation techniques are heavily reliant on EAM systems, which invasively create 3-dimensional reconstructions of ventricular geometry (Carto, Biosense Webster, Inc; NAVX, St Jude Medical; Rhythmia Mapping, Boston Scientific Inc). Relying solely on EAM is associated with important limitations because EAM systems do not provide true anatomic imaging but rather derived 3-dimensional reconstructions from catheter–electrode contact at the myocardial surface. The extrapolation of data based on catheter surface contact to the entire thickness of the ventricular myocardium has the potential to generate inaccurate data on scar characteristics. Additional errors may arise because of inconsistencies in catheter contact and the confounding effects of far-field signals from distant sites.

Overall, depending on the source of error, EAM systems have the potential to under- or overestimate the extent of scar and arrhythmogenic substrate. To overcome these limitations, interest has recently increased in real-time integration of pre- or intraprocedural imaging into EAM systems to guide VT ablation procedures. Integration of imaging data allows more accurate definition of the extent and distribution of the arrhythmogenic substrate. Furthermore, image integration provides intricate anatomic detail in regions that may be difficult to access with catheters.

Integration of CMR

Multiple image-integration studies have investigated the accuracy of EAM for scar definition by correlating

CMR- and EAM-defined scar (Table II in the online-only Data Supplement). Although the results have been variable across studies, a number have demonstrated mismatch between the 2 modalities.[61–65] These reports underscore the value of integrating EAM and LGE-CMR for comprehensive scar characterization, particularly in the context of defining infarct border zones, nontransmural scars, and small subepicardial scars.[62] A procedural example illustrating the added value of LGE-CMR integration and the limitations of EAM is shown in Figure 2.

In addition to enhancing accuracy of scar definition, LGE-CMR image integration has the potential to facilitate more targeted approaches to VT ablation. Ablation strategies focusing on CMR-defined scars are supported by studies that have consistently demonstrated that critical VT isthmuses are located within LGE areas.[66–69] In recent years, in an attempt to refine targeted VT ablation strategies further, studies have focused on identifying specific scar regions that harbor critical VT isthmuses. Scar regions with increased transmurality, scar border zones, and regions at the scar core–border zone transition have been identified as potential targets.[70–72]

Overall, CMR integration is a potentially powerful adjunct to voltage mapping to comprehensively localize scar and could be used to focus substrate mapping. However, the ability of CMR to preemptively identify catheter ablation targets remains uncertain.

Integration of MDCT

MDCT represents a valuable alternative for imaging integration among patients in whom CMR is contraindicated or of suboptimal quality because of ICD-related artifacts. A number of MDCT image characteristics can be used for scar definition, including wall thinning, hypoattenuation (because of fatty metaplasia), decreased perfusion, and hyperattenuation.[17–19] Several studies have assessed the agreement between scar defined by MDCT and that defined by EAM systems (Table II in the online-only Data Supplement). Although all of the aforementioned MDCT scar definition techniques have demonstrated a good correlation with EAM-defined scar in patients with ICM, the correlation in patients with NICMs is less robust.[17–19,73] In addition to scar correlation, these studies have demonstrated that the electrophysi-

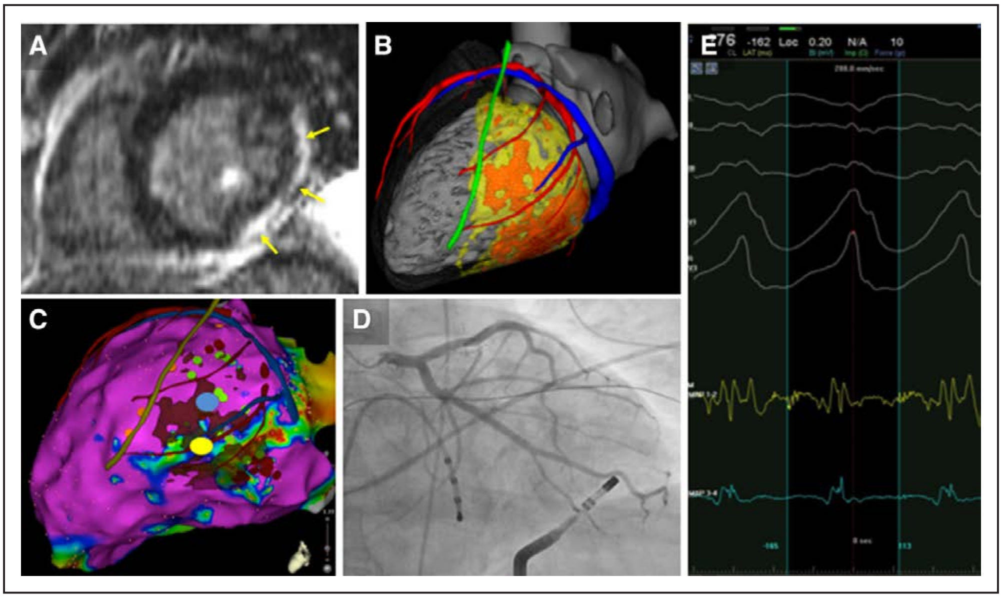

Figure 2. Example of image integration to assist ventricular tachycardia ablation in a case of myocarditis.
A, Lateral and inferior LV scar on CMR (arrows). **B,** Patient-specific 3-dimensional model built from merged CT (anatomy) and MRI (scar) data. Cardiac chambers (gray), coronary arteries, and veins (in red and blue, respectively), left phrenic nerve (green), as segmented from CT, and dense scar and gray zone (in orange and yellow, respectively) as segmented from CMR. **C,** Epicardial bipolar voltage map with merged imaging model. Voltage mapping (color-coded from purple to red) underestimates substrate extent as compared with imaging. Fractionated and late potentials (green dots) are identified in normal voltage areas. Middiastolic potentials (yellow and blue signals in **E**) are recorded during VT on an epicardial lateral left ventricular site (yellow dot in **C**). This potential target for epicardial ablation is far enough from the left phrenic nerve path derived from imaging (green line in **C**), which accurately matches sites of phrenic capture (orange dots in **C**). However, CT demonstrates proximity of this site to a marginal branch of circumflex artery on the registered imaging model. Confirmatory coronary angiography (**D** and Movie I in online-only Data Supplement) demonstrates contact between the tip of the ablation catheter and the coronary artery. Ablation was thus performed on a different site of the VT isthmus (blue dot in **C**), resulting in successful VT termination. CMR indicates cardiac magnetic resonance; CT, computed tomography; LV, left ventricle; MRI, magnetic resonance imaging; and VT, ventricular tachycardia.

ological VT substrate in patients with ICM and NICM is located within or in close proximity to MDCT-defined scar.[17,19,73] These findings indicate that MDCT image integration may also facilitate more targeted ablation.

MDCT is the most effective imaging technique for defining detailed cardiac anatomy, including the coronary arterial and venous systems, valve apparatus, left phrenic nerve, and epicardial fat and calcification. The ability to display coronary arteries and the left phrenic nerve using MDCT is particularly relevant for patients undergoing epicardial VT ablation procedures because it obviates the need for repeated coronary angiography and phrenic pacing maneuvers.[65] Examples illustrating the importance of imaging coronary arteries during epicardial ablation and the use of MDCT in this context are included, respectively, in Figure 2 and Movie I in the online-only Data Supplement. The ability to visualize epicardial fat is also important for epicardial procedures because voltage mapping may be unreliable, and epicardial ablation may be ineffective in these regions.[74] MDCT is also valuable for ablation of VT originating from areas with complex anatomy. An example of MDCT integration for the ablation of papillary muscle VT is shown in Figure 3.

Integration of Nuclear Imaging

Nuclear image-integration studies (^{201}Tl SPECT and PET/CT) have reported variable results in terms of the correlation with EAM-defined scar (Table II in the online-only Data Supplement).[75,76] Although some reports have demonstrated that EAM underestimates scar area, others have reported that regions with normal metabolic activity are incorrectly defined as scar by EAM.[75,77] In addition to metabolic activity, nuclear imaging of sympathetic innervation with ^{123}I-*m*IBG SPECT has demonstrated that areas of denervation are larger than EAM-defined scar.[78] Overall, these studies suggest that nuclear image integration is useful for more comprehensive scar characterization.

Targeting scar defined by nuclear imaging techniques potentially represents an effective VT ablation strategy. Isthmuses that are critical to the maintenance of VT have been demonstrated to be located within or in close proximity to ^{201}Tl SPECT– and PET/CT-defined scar.[77,79] Interestingly, PET/CT has been reported to identify channels of metabolically active surviving tissue within scar that are not identified by voltage mapping.[75] Furthermore, one third of VTs originating from sites of normal voltage on EAM are located in areas of denervation on SPECT imaging.[78]

Although the above nuclear image integration studies in small patient cohorts have demonstrated that nuclear imaging provides incremental information on the arrhythmogenic substrate, the utility of the technique is not widespread. A major limitation of nuclear imaging techniques in this context is that they do not provide

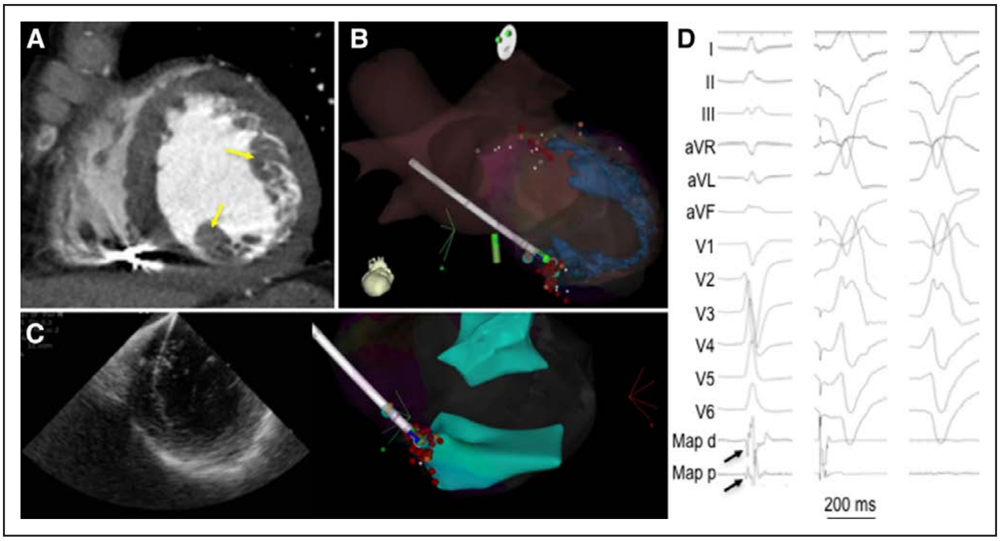

Figure 3. Example of combining intracardiac echocardiography and CT to assist catheter navigation in a case with papillary muscle PVC.
A, CT demonstrating detailed anatomy of the mitral subvalvular apparatus (arrows). **B,** CT-derived anatomy of the cardiac chambers (purple surface) and papillary muscles (blue surface) integrated in the CARTO system to assist catheter navigation. **C,** Intracardiac echocardiography providing real-time assessment of catheter tip motion with respect to posteromedial papillary muscle. **D,** Purkinje potentials preceding the ventricular electrogram recorded on the posteromedial papillary muscle during sinus rhythm (first column in **D**). Pace mapping at this site (middle column in **D**) reproduced the clinical PVC morphology (third column in **D**). Ablation at this site with continuous monitoring of catheter and papillary muscle motion on intracardiac echo resulted in successful elimination of Purkinje potentials and loss of arrhythmia inducibility. Movies illustrating catheter motion within CT and echo data can be found in Movies II and III in the online-only Data Supplement. CT indicates computed tomography; and PVC, premature ventricular complex.

sufficient anatomic detail and commonly require integration with other imaging modalities.

Integration of Intracardiac Echocardiography

Intracardiac echocardiography (ICE) utilizes ultrasound catheters to generate 3-dimensional representations of ventricular anatomy that can be integrated in real time with EAM. In patients with scar-related VT, ICE defines the location and extent of scar based on the identification of thinned, akinetic, or dyskinetic segments with increased echo density. A number of studies have reported a robust correlation between scar area identified by ICE and that defined by EAM.[80,81] Furthermore, based on scar echo density, scar core has been differentiated from scar border zone as defined by EAM.[81] Of note, ICE-defined scar characterization has also been validated against LGE-CMR and MDCT.[80] Despite the observed correlation between ICE- and EAM-defined scar, the technique is less effective for detailed scar characterization when compared with MDCT and CMR.

A major advantage of ICE imaging compared with the other imaging modalities is that it provides dynamic real-time imaging of ventricular anatomy, catheter contact, and catheter orientation, and it is not limited by registration issues.[82] The technique is therefore particularly valuable for VTs arising from sites with complex anatomy, such as periaortic VT and papillary muscle VT. An example of ICE integration to assist catheter ablation of papillary muscle VT is shown in Figure 3 and Movies II and III in the online-only Data Supplement.

Imaging to Assess Ablation Lesions

The advances in imaging technology discussed thus far have focused on precise characterization of the VT substrate to facilitate targeted VT ablation. Another important area of development is the use of noninvasive imaging techniques for direct visualization of lesion characteristics, which may enhance efficacy of VT ablation. The development of these techniques may also play an important role in determining the optimal ablation strategy. Current approaches for as-

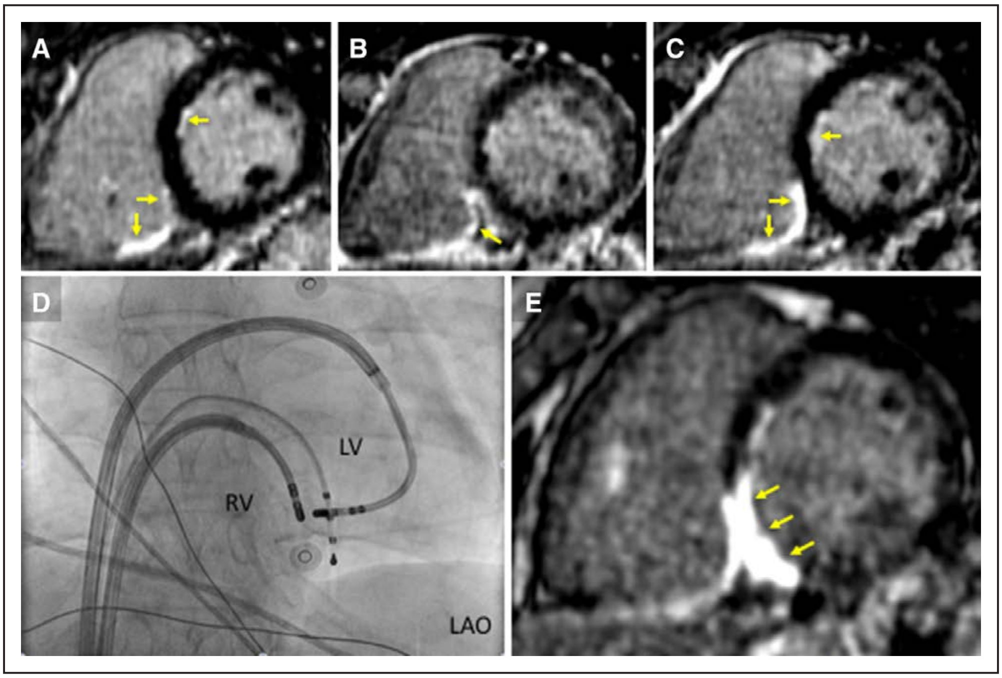

Figure 4. Imaging to assess scarring after ablation in a case of idiopathic septal VT with multiple previous failed ablations.

A, Late gadolinium-enhanced CMR demonstrating subendocardial scar from prior failed ablations on both sides of the septum and on inferior RV (arrows). Septal thickness is preserved and septal scar is nontransmural. In an attempt to maximize scar transmurality, higher energy ablation was performed, resulting in an uncomplicated steam pop. **B,** CMR image on day 1 after steam pop demonstrating an intramural hematoma close to posterior RV insertion (arrow), which did not translate into increased lesion transmurality. **C,** Repeat CMR (2 years later) demonstrated complete resolution of the intramural hematoma and persisting subendocardial scar. **D,** Because of arrhythmia recurrence, bipolar ablation was performed using ablation catheters on either side of the septum, as guided by fluoroscopy and electroanatomical mapping with image integration. This procedure was successful in eliminating the arrhythmia. **E,** CMR image at 3 months after successful bipolar ablation showed dense transmural scar within the septum (arrows in **E**). CMR indicates cardiac magnetic resonance; LAO, left-anterior-oblique view; RV, right ventricle; and VT, ventricular tachycardia.

sessing lesion characteristics focus on the catheter–tissue interface and are therefore less effective for the assessment of lesion depth, which may be particularly relevant for VT originating from deep intramural substrates.

Post Procedure Imaging of Ablation Lesions

CMR offers excellent soft tissue visualization and therefore lends itself to the characterization of lesion characteristics. In animal models, LGE-CMR–defined lesion characteristics demonstrate a high degree of correlation with histologically defined lesions.[83] A number of human studies have also demonstrated that post procedure LGE-CMR is an effective imaging modality for the characterization of lesion size and extent of transmurality.[84,85] Post-ablation scar transmurality on LGE-CMR has been reported to predict VT ablation success for intramural VT substrates.[84] An example illustrating the use of post-ablation LGE-CMR to document lesion transmurality is shown in Figure 4.

Tissue changes after VT ablation have also been characterized using nuclear imaging techniques such as ^{123}I-*m*IBG SPECT. VT ablation has been reported to cause dynamic changes in autonomic innervation, which, it could be speculated, influences arrhythmic risk.[86] Thus, characterization of ablation lesions using imaging might help understanding ablation failure and lead to development of alternate approaches for resistant substrates.

Real-Time Imaging of Ablation Lesions

The ultimate goal of imaging ablation lesions is to provide real-time feedback on lesion characteristics. Real-time lesion imaging has multiple potential advantages, including the availability of detailed anatomic information in real time, the ability to guide catheter manipulation with minimal fluoroscopic exposure, and feedback on both lesion characteristics and spatial correlation between lesions and predefined ablation targets. Real-time integration also overcomes potential confounding effects of performing noninvasive imaging and EAM at different time points, particularly in terms of registration.

Significant efforts are currently underway to enable real-time CMR-based assessment of lesion formation. Potential strategies for acute assessment of lesion formation include monitoring of tissue edema (on T_2-

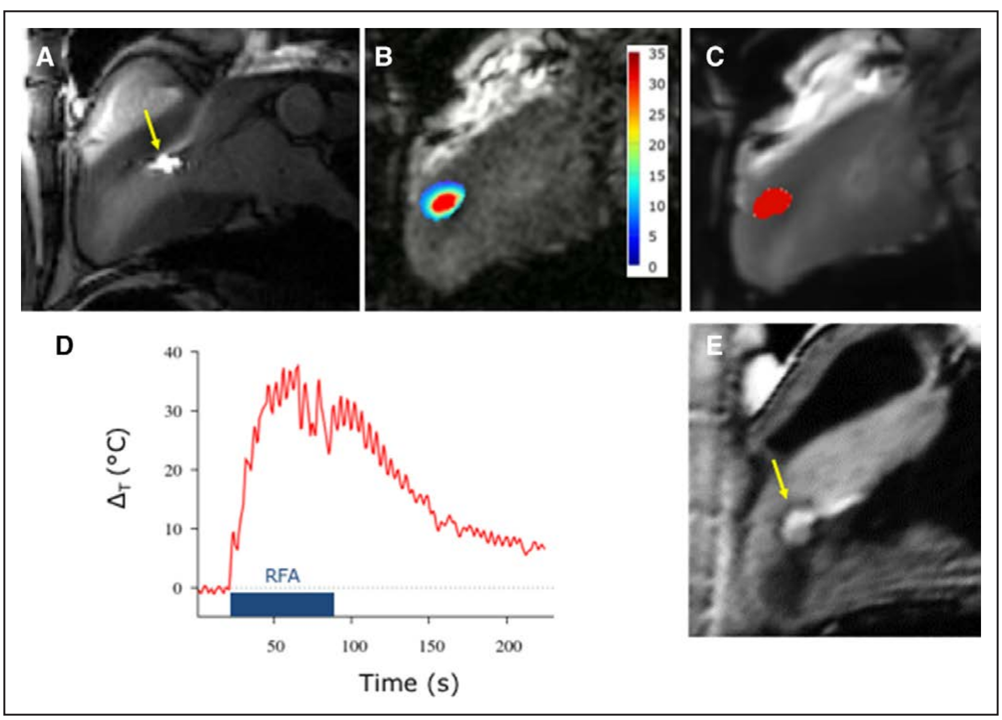

Figure 5. Use of CMR to monitor lesion formation in real time.
A, Interactive imaging with active slice tracking on the catheter tip is used to navigate the catheter toward the targeted position (in a sheep model). The catheter appears in hyposignal with a bright spot at its tip where an MR coil is present (arrow). **B,** RF ablation under real-time MR thermometry (1 temperature measurement per heart beat), with the temperature increase above body temperature being displayed in real time within the tissue. **C,** A computed thermal dose image, with pixels colored in red indicating that a lethal cumulative thermal dose has been reached. **D,** On each pixel, the temperature curve can be plotted against time (blue bar indicates RF delivery). **E,** Resulting lesion assessed immediately after ablation using T_1-weighted imaging without contrast agent (arrow). CMR indicates cardiac magnetic resonance; MR, magnetic resonance; and RF, radiofrequency.

weighted CMR images), documentation of intramural low flow or hematoma (on T_1-weighted CMR images), and real-time measurement of tissue temperature during radiofrequency delivery (Figure 5). Studies in animal models have demonstrated that these approaches are feasible.[87] It is important to emphasize, however, that before a real-time MR-guided electrophysiology suite can be developed for clinical use, significant technological challenges need to be addressed. Examples include MR compatibility of electrophysiology catheters, appropriate processing of electrophysiology signals to preserve diagnostic quality, and practical improvements to simplify cardioversion in an MR environment.[87,88]

FUTURE PERSPECTIVES

Noninvasive Electrophysiological Assessment With Electrocardiographic Imaging (ECGI)

Until recently, detailed characterization of ventricular activation patterns during VT has largely been restricted to patients undergoing invasive ablation procedures. Noninvasive ECGI has emerged as a promising technique that has the potential to overcome this restriction. ECGI uses advanced mathematical algorithms to reconstruct epicardial activation maps from a large number of unipolar body surface potentials.[89] ECGI has a number of important potential advantages. In addition to obviating the need for an invasive procedure, it has the potential to map activation patterns during hemodynamically unstable ventricular arrhythmias as it provides simultaneous whole-heart assessment of cardiac activation.

In animal models, ECGI has been reported to generate images of reentrant VT circuits, which includes detailed delineation of slowly conducting isthmuses.[90,91] A case illustrating the use of ECGI to noninvasively assess VT mechanism in a human subject is shown in Figure 6 and Movies IV and V in the online-only Data Supplement. Despite ECGI's early promise, however, potential challenges must be addressed before it can be used routinely in patients with scar-related VT. For instance, current body surface mapping algorithms may not have suf-

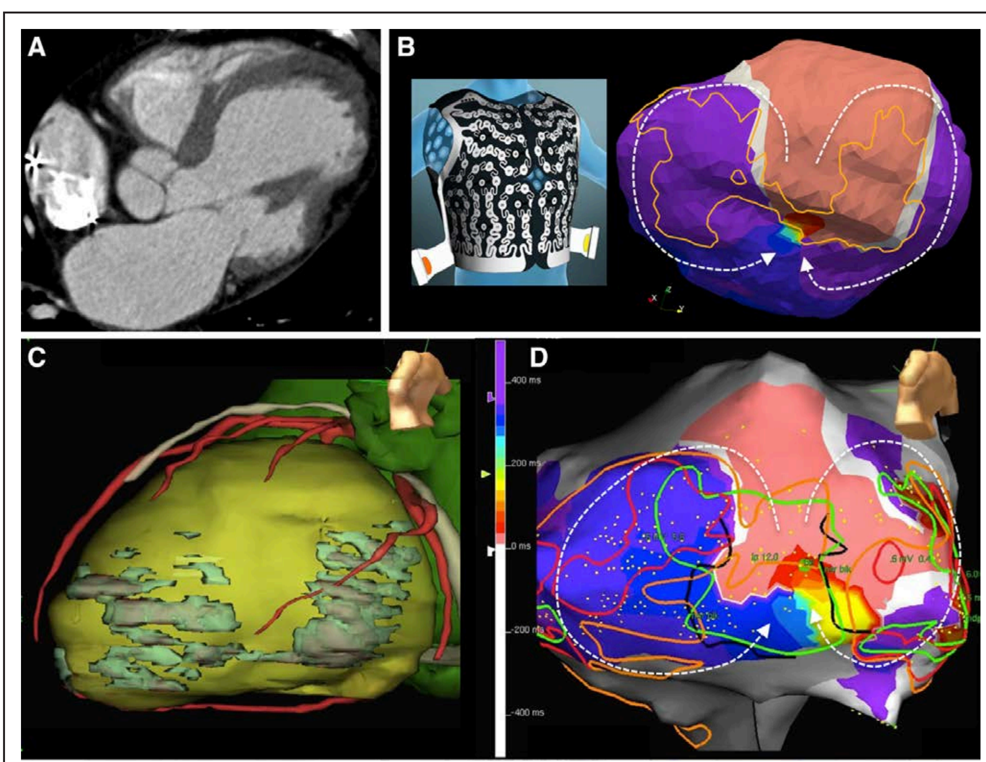

Figure 6. Example of ECGI mapping to noninvasively assess VT mechanism in a case of nonischemic dilated cardiomyopathy.

A, ECG-gated contrast-enhanced CT shows LV dilatation and 2 areas of severe wall thinning separated by an anatomic channel of preserved thickness on lateral LV wall (arrows). **B,** ECGI during VT using a multielectrode system demonstrating a figure-of-8-type activation with an isthmus matching the CT-defined anatomic channel. **C,** Electroanatomical mapping using the Ensite system and with the integration of anatomy and scar data as segmented from imaging. **D,** Epicardial activation mapping during VT confirmed the VT mechanism suspected from noninvasive imaging. Movies IV and V in the online-only Data Supplement illustrate VT activation as assessed by ECGI and contact mapping, respectively. CT indicates computed tomography; ECGI, electrocardiographic imaging; and VT, ventricular tachycardia.

ficient resolution to differentiate between low-amplitude signals at critical isthmus sites and high-amplitude far-field signals. Efforts are currently ongoing to increase the resolution of ECGI mapping in this context.

Image-Based Electrophysiological Computational Modeling

A potentially powerful emerging technique for noninvasive characterization of VT mechanisms involves the simulation of ventricular activation patterns using patient-specific, imaging-derived computational modeling. Multimodality imaging techniques provide detailed patient-specific data on ventricular geometry and 3-dimensional scar architecture. Incorporating these data into computational biophysical cardiac models has the potential to predict arrhythmia mechanisms in silico. A series of proof-of-concept studies have suggested that image-based modeling could be used to predict the arrhythmogenic substrate, potential VT circuits, and future arrhythmic events.[92,93] An example of MDCT-based simulation of post-infarction VT is shown in Figure 7 and Movie VI in the online-only Data Supplement.

Despite encouraging initial results, integration of imaging information into computational models is associated with multiple challenges, including image

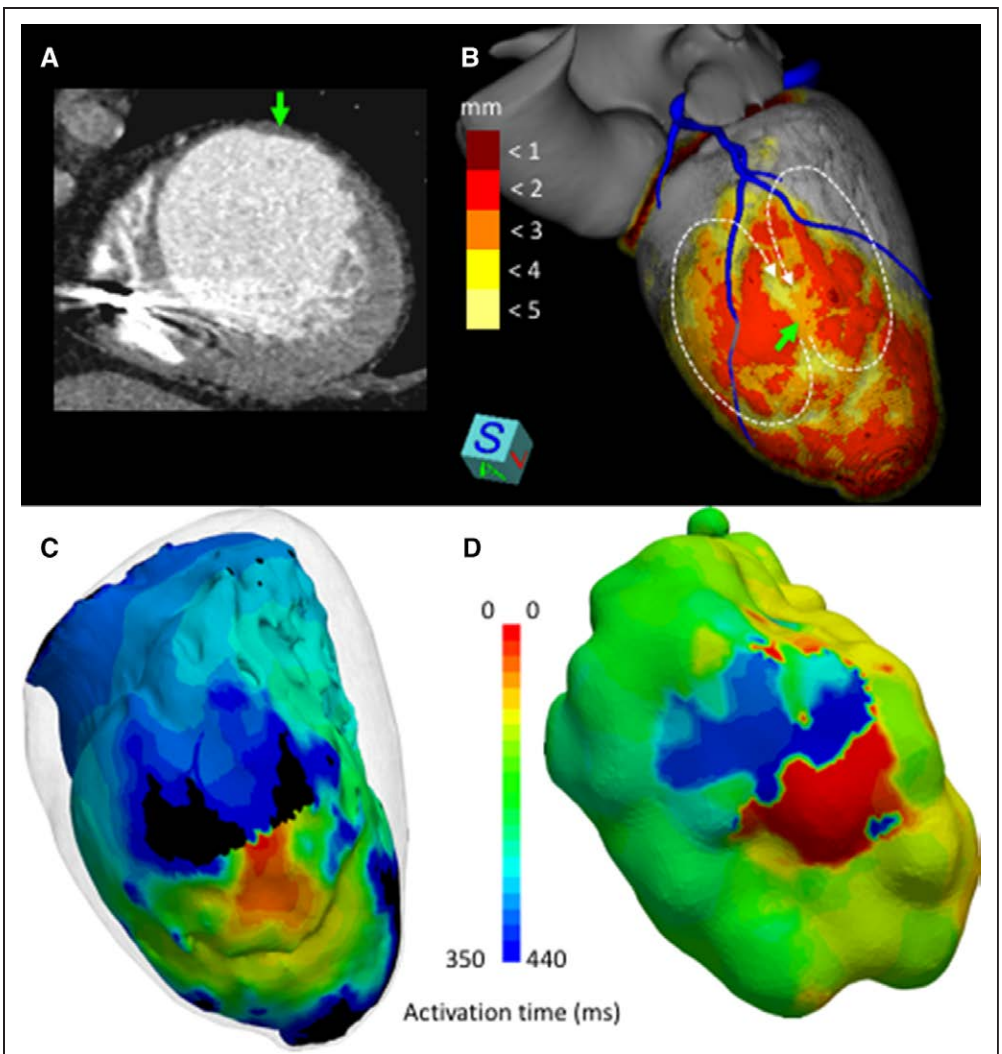

Figure 7. Example of image-based biophysical modeling to predict VT mechanism in a case of ischemic cardiomyopathy.

A, CT to assess cardiac anatomy and analyze substrate heterogeneity using wall thickness mapping. **B,** An anatomic channel of relatively preserved thickness between 2 areas of severe thinning is seen on anterior LV (green arrows in **A** and **B**). CT data are used to personalize a 3-dimensional computationally derived model (Eikonal model) of cardiac electrophysiology using regional wall thickness to estimate conduction properties within the infarct. This model is paced on the channel in front of a unidirectional block, resulting in a simulated activation sequence (**C**) that accurately matches the VT activation assessed by contact in the Rhythmia system (**D**). Activation sequences obtained from simulation and contact mapping are shown in Movie VI in the online-only Data Supplement. CT indicates computed tomography; and VT, ventricular tachycardia.

segmentation to extract the most relevant imaging features, registration between generic models and patient-specific anatomic variations, and translation of imaging features into electrophysiological properties (model parameters). Studies are ongoing to further validate model simulations against detailed VT mapping data and to reduce computational data processing times to make modeling systems compatible with clinical workflows.

Improvements of Structural Imaging

A developing strategy for image-guided therapy in patients with VT involves direct high-resolution imaging of VT isthmuses within scar. In animal models, ex vivo CMR has been reported to delineate VT isthmuses with near histological accuracy.[94] Studies in humans have demonstrated that gray zone corridors within dense scar potentially correlate with VT isthmuses.[95,96] However, limitations of current CMR imaging, including insufficient spatial resolution, inability to identify interstitial fibrosis, and lack of consistency relating to methods used to assess scar heterogeneity, have limited its utility for isthmus imaging.[4,34,42,43] In the future, the development of more advanced imaging techniques such as molecular CMR, using contrast agents that target specific extracellular matrix proteins, may be more effective for distinguishing between different scar components.[97]

MDCT is also emerging as a potentially effective technique for direct visualization of VT isthmuses. The superior spatial resolution of MDCT can be exploited for detailed characterization of scar heterogeneity. Specifically, distinguishing between areas with severe and moderate wall thinning has the potential to identify isthmuses within dense scar. Although MDCT-derived wall thickness mapping has not been validated against reference techniques such as LGE-CMR, the approach has demonstrated convincing electrophysiological correlates.[17] Recently, preliminary results from our group (H. Cochet, MD, unpublished data, 2017) and others have demonstrated that channels with relatively preserved wall thickness crossing severely thinned areas colocalize with critical VT isthmuses and also host a higher density of late potentials (Figure 8 and Movie VII in the online-only Data Supplement).

Multimodality Approaches

Current imaging techniques have their own individual strengths and limitations. An important area of potential development involves combining multiple imaging modalities to exploit the relative strengths of each. In a recent proof-of-concept study, Cochet and colleagues[98] used a multimodality integrative approach involving MDCT or LGE-CMR and ECGI. The approach noninvasively defined the arrhythmia mechanism, identified the critical isthmuses, and defined the relationship of the isthmus to the structural VT substrate. An example of combined MDCT and ECGI assessment in a patient with scar-related VT is illustrated in Figure 6. In the future, expanding on these studies could potentially lead to the development of 1-stop hybrid imaging techniques that simultaneously characterize intricate scar architecture, cardiac metabolism, cardiac sympathetic innervation, and cardiac electric activation patterns.

Conclusions

Over the past 2 decades, the role of cardiac imaging in patients with VT has progressed from making relatively crude measurements of left ventricular ejection fraction to defining intricate details of scar architecture and providing complementary information on cardiac metabolism, innervation, and, perhaps most importantly,

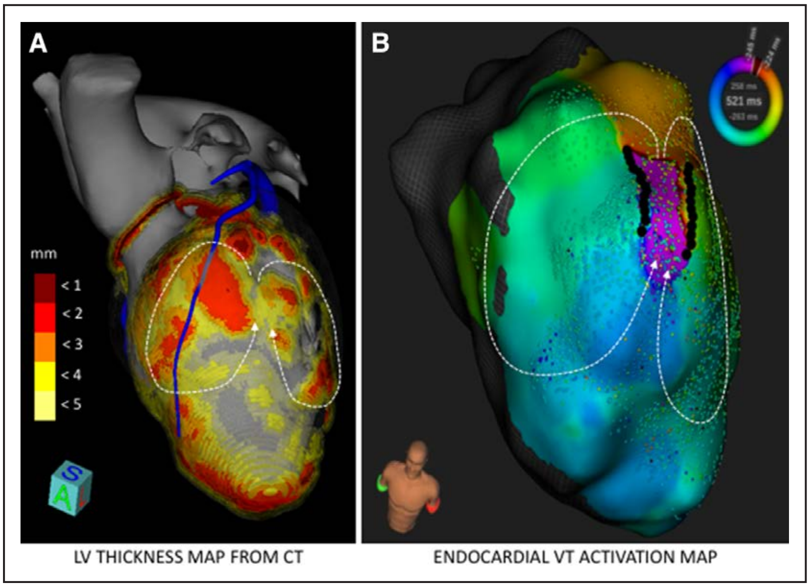

Figure 8. Example of prediction of a ventricular tachycardia circuit from MDCT imaging in a case of ischemic cardiomyopathy.
A, ECG-gated contrast-enhanced CT delineating myocardial scar (identified as areas of wall thinning <5 mm). Wall thickness mapping shows an anatomic channel of relatively preserved thickness between 2 areas of severe thinning on the anterior left ventricle. **B,** High-density endocardial activation map during VT (using the Rhythmia system), demonstrating a colocalization between the imaging-defined anatomic channel and the critical VT isthmus. Movie VII in the online-only Data Supplement illustrates the VT activation map. CT indicates computed tomography; MDCT, multidetector cardiac CT; and VT, ventricular tachycardia.

 Circulation. 2017;136:2491–2507. DOI: 10.1161/CIRCULATIONAHA.117.029349

electric activation. In the future, the pace of advance in imaging technology has the potential to revolutionize management of patients with scar-related VT, by both refining risk stratification and providing predefined direct targets for catheter ablation therapy. However, the translation of technological advances from research studies into routine clinical practice will require larger collaborative efforts.

ACKNOWLEDGMENTS

We thank Bruno Quesson, PhD; Valery Ozenne, PhD; Nicolas Cedilnik, MSc; Ghassen Cheniti, MD; and Masateru Takigawa, MD, for their contribution to the figures in the manuscript. We also thank Dhiraj Gupta, MD; Mark Hall, MD; Nicolas Derval, MD; and Derick Todd, MD, for their valuable edits to the manuscript.

SOURCES OF FUNDING

This work was supported by l'Agence Nationale de la Recherche (grants ANR-10-IAHU-04 and ANR-11-EQPX-0030) and the European Research Council (grant 715093).

DISCLOSURES

Dr Sacher has received consulting fees and speaking honoraria from Boston Scientific, Biosense Webster, St Jude Medical, and Medtronic. Dr Jaïs has received consulting fees and speaking honoraria from and is part of the Scientific Advisory Board of Biosense Webster and St Jude Medical. Drs Haïssaguerre and Jaïs are stockowners of and Dr Dubois is a paid consultant to CardioInsight Inc. The other authors report no conflicts.

AFFILIATIONS

Department of Cardiac Electrophysiology, Liverpool Heart and Chest Hospital, UK (S.M.). L'Institut de Rythmologie et Modélisation Cardiaque (LIRYC), Centre Hospitalier Universitaire (CHU) de Bordeaux, France (F.S., R.D., M.H., P.J., H.C.). Inria Sophia Antipolis, Sophia Antipolis-Méditerranée, France (M.S.). Division of Cardiology, University of Michigan, Ann Arbor (F.B.).

FOOTNOTES

The online-only Data Supplement is available with this article at http://circ.ahajournals.org/lookup/suppl/doi:10.1161/CIRCULATIONAHA.117.029349/-/DC1.

Circulation is available at http://circ.ahajournals.org.

REFERENCES

1. Kuck KH, Schaumann A, Eckardt L, Willems S, Ventura R, Delacrétaz E, Pitschner HF, Kautzner J, Schumacher B, Hansen PS; VTACH Study Group. Catheter ablation of stable ventricular tachycardia before defibrillator implantation in patients with coronary heart disease (VTACH): a multicentre randomised controlled trial. *Lancet*. 2010;375:31–40. doi: 10.1016/S0140-6736(09)61755-4.
2. Priori SG, Blomström-Lundqvist C, Mazzanti A, Blom N, Borggrefe M, Camm J, Elliott PM, Fitzsimons D, Hatala R, Hindricks G, Kirchhof P, Kjeldsen K, Kuck KH, Hernandez-Madrid A, Nikolaou N, Norekvål TM, Spaulding C, Van Veldhuisen DJ. 2015 ESC Guidelines for the management of patients with ventricular arrhythmias and the prevention of sudden cardiac death: the task force for the management of patients with ventricular arrhythmias and the prevention of sudden cardiac death of the European Society of Cardiology (ESC). Endorsed by: Association for European Paediatric and Congenital Cardiology (AEPC). *Eur Heart J*. 2015;36:2793–2867. doi: 10.1093/eurheartj/ehv316.
3. Nagel E, Lehmkuhl HB, Bocksch W, Klein C, Vogel U, Frantz E, Ellmer A, Dreysse S, Fleck E. Noninvasive diagnosis of ischemia-induced wall motion abnormalities with the use of high-dose dobutamine stress MRI: comparison with dobutamine stress echocardiography. *Circulation*. 1999;99:763–770.
4. Aljaroudi WA, Flamm SD, Saliba W, Wilkoff BL, Kwon D. Role of CMR imaging in risk stratification for sudden cardiac death. *JACC Cardiovasc Imaging*. 2013;6:392–406. doi: 10.1016/j.jcmg.2012.11.011.
5. Haaf P, Garg P, Messroghli DR, Broadbent DA, Greenwood JP, Plein S. Cardiac T1 mapping and cxtracellular volume (ECV) in clinical practice: a comprehensive review. *J Cardiovasc Magn Reson*. 2016;18:89. doi: 10.1186/s12968-016-0308-4.
6. Luetkens JA, Homsi R, Sprinkart AM, Doerner J, Dabir D, Kuetting DL, Block W, Andrié R, Stehning C, Fimmers R, Gieseke J, Thomas DK, Schild HH, Naehle CP. Incremental value of quantitative CMR including parametric mapping for the diagnosis of acute myocarditis. *Eur Heart J Cardiovasc Imaging*. 2016;17:154–161. doi: 10.1093/ehjci/jev246.
7. Gersh BJ, Maron BJ, Bonow RO, Dearani JA, Fifer MA, Link MS, Naidu SS, Nishimura RA, Ommen SR, Rakowski H, Seidman CE, Towbin JA, Udelson JE, Yancy CW; American College of Cardiology Foundation/American Heart Association Task Force on Practice Guidelines; American Association for Thoracic Surgery; American Society of Echocardiography; American Society of Nuclear Cardiology; Heart Failure Society of America; Heart Rhythm Society; Society for Cardiovascular Angiography and Interventions; Society of Thoracic Surgeons. 2011 ACCF/AHA guideline for the diagnosis and treatment of hypertrophic cardiomyopathy: executive summary: a report of the American College of Cardiology Foundation/American Heart Association Task Force on Practice Guidelines. *Circulation*. 2011;124:2761–2796. doi: 10.1161/CIR.0b013e318223e230.
8. Marcus FI, McKenna WJ, Sherrill D, Basso C, Bauce B, Bluemke DA, Calkins H, Corrado D, Cox MG, Daubert JP, Fontaine G, Gear K, Hauer R, Nava A, Picard MH, Protonotarios N, Saffitz JE, Sanborn DM, Steinberg JS, Tandri H, Thiene G, Towbin JA, Tsatsopoulou A, Wichter T, Zareba W. Diagnosis of arrhythmogenic right ventricular cardiomyopathy/dysplasia: proposed modification of the task force criteria. *Circulation*. 2010;121:1533–1541. doi: 10.1161/CIRCULATIONAHA.108.840827.
9. White JA, Fine NM, Gula L, Yee R, Skanes A, Klein G, Leong-Sit P, Warren H, Thompson T, Drangova M, Krahn A. Utility of cardiovascular magnetic resonance in identifying substrate for malignant ventricular arrhythmias. *Circ Cardiovasc Imaging*. 2012;5:12–20. doi: 10.1161/CIRCIMAGING.111.966085.
10. Roguin A, Schwitter J, Vahlhaus C, Lombardi M, Brugada J, Vardas P, Auricchio A, Priori S, Sommer T. Magnetic resonance imaging in individuals with cardiovascular implantable electronic devices. *Europace*. 2008;10:336–346. doi: 10.1093/europace/eun021.
11. Nazarian S, Hansford R, Roguin A, Goldsher D, Zviman MM, Lardo AC, Caffo BS, Frick KD, Kraut MA, Kamel IR, Calkins H, Berger RD, Bluemke DA, Halperin HR. A prospective evaluation of a protocol for magnetic resonance imaging of patients with implanted cardiac devices. *Ann Intern Med*. 2011;155:415–424. doi: 10.7326/0003-4819-155-7-201110040-00004.
12. Gold MR, Sommer T, Schwitter J, Al Fagih A, Albert T, Merkely B, Peterson M, Ciuffo A, Lee S, Landborg L, Cerkvenik J, Kanal E; Evera MRI Study Investigators. Full-body MRI in patients with an implantable cardioverter-defibrillator: primary results of a randomized study. *J Am Coll Cardiol*. 2015;65:2581–2588. doi: 10.1016/j.jacc.2015.04.047.
13. Mesubi O, Ahmad G, Jeudy J, Jimenez A, Kuk R, Saliaris A, See V, Shorofsky S, Dickfeld T. Impact of ICD artifact burden on late gadolinium enhancement cardiac MR imaging in patients undergoing ventricular tachycardia ablation. *Pacing Clin Electrophysiol*. 2014;37:1274–1283. doi: 10.1111/pace.12405.
14. Matsunari I, Taki J, Nakajima K, Tonami N, Hisada K. Myocardial viability assessment using nuclear imaging. *Ann Nucl Med*. 2003;17:169–179.

15. Tung R, Bauer B, Schelbert H, Lynch JP III, Auerbach M, Gupta P, Schiepers C, Chan S, Ferris J, Barrio M, Ajijola O, Bradfield J, Shivkumar K. Incidence of abnormal positron emission tomography in patients with unexplained cardiomyopathy and ventricular arrhythmias: the potential role of occult inflammation in arrhythmogenesis. *Heart Rhythm*. 2015;12:2488–2498. doi: 10.1016/j.hrthm.2015.08.014.
16. Budoff MJ, Achenbach S, Blumenthal RS, Carr JJ, Goldin JG, Greenland P, Guerci AD, Lima JA, Rader DJ, Rubin GD, Shaw LJ, Wiegers SE; American Heart Association Committee on Cardiovascular Imaging and Intervention; American Heart Association Council on Cardiovascular Radiology and Intervention; American Heart Association Committee on Cardiac Imaging, Council on Clinical Cardiology. Assessment of coronary artery disease by cardiac computed tomography: a scientific statement from the American Heart Association Committee on Cardiovascular Imaging and Intervention, Council on Cardiovascular Radiology and Intervention, and Committee on Cardiac Imaging, Council on Clinical Cardiology. *Circulation*. 2006;114:1761–1791. doi: 10.1161/CIRCULATIONAHA.106.178458.
17. Komatsu Y, Cochet H, Jadidi A, Sacher F, Shah A, Derval N, Scherr D, Pascale P, Roten L, Denis A, Ramoul K, Miyazaki S, Daly M, Riffaud M, Sermesant M, Relan J, Ayache N, Kim S, Montaudon M, Laurent F, Hocini M, Haïssaguerre M, Jaïs P. Regional myocardial wall thinning at multidetector computed tomography correlates to arrhythmogenic substrate in postinfarction ventricular tachycardia: assessment of structural and electrical substrate. *Circ Arrhythm Electrophysiol*. 2013;6:342–350. doi: 10.1161/CIRCEP.112.000191.
18. Tian J, Jeudy J, Smith MF, Jimenez A, Yin X, Bruce PA, Lei P, Turgeman A, Abbo A, Shekhar R, Saba M, Shorofsky S, Dickfeld T. Three-dimensional contrast-enhanced multidetector CT for anatomic, dynamic, and perfusion characterization of abnormal myocardium to guide ventricular tachycardia ablations. *Circ Arrhythm Electrophysiol*. 2010;3:496–504. doi: 10.1161/CIRCEP.109.889311.
19. Esposito A, Palmisano A, Antunes S, Maccabelli G, Colantoni C, Rancoita PMV, Baratto F, Di Serio C, Rizzo G, De Cobelli F, Della Bella P, Del Maschio A. Cardiac CT with delayed enhancement in the characterization of ventricular tachycardia structural substrate: relationship between CT-segmented scar and electro-anatomic mapping. *JACC Cardiovasc Imaging*. 2016;9:822–832. doi: 10.1016/j.jcmg.2015.10.024.
20. Epstein AE, DiMarco JP, Ellenbogen KA, Estes NA III, Freedman RA, Gettes LS, Gillinov AM, Gregoratos G, Hammill SC, Hayes DL, Hlatky MA, Newby LK, Page RL, Schoenfeld MH, Silka MJ, Stevenson LW, Sweeney MO; American College of Cardiology Foundation; American Heart Association Task Force on Practice Guidelines; Heart Rhythm Society. 2012 ACCF/AHA/HRS focused update incorporated into the ACCF/AHA/HRS 2008 guidelines for device-based therapy of cardiac rhythm abnormalities: a report of the American College of Cardiology Foundation/American Heart Association Task Force on Practice Guidelines and the Heart Rhythm Society. *Circulation*. 2013;127:e283–e352. doi: 10.1161/CIR.0b013e318276ce9b.
21. Dawson DK, Hawlisch K, Prescott G, Roussin I, Di Pietro E, Deac M, Wong J, Frenneaux MP, Pennell DJ, Prasad SK. Prognostic role of CMR in patients presenting with ventricular arrhythmias. *JACC Cardiovasc Imaging*. 2013;6:335–344. doi: 10.1016/j.jcmg.2012.09.012.
22. Gulati A, Jabbour A, Ismail TF, Guha K, Khwaja J, Raza S, Morarji K, Brown TD, Ismail NA, Dweck MR, Di Pietro E, Roughton M, Wage R, Daryani Y, O'Hanlon R, Sheppard MN, Alpendurada F, Lyon AR, Cook SA, Cowie MR, Assomull RG, Pennell DJ, Prasad SK. Association of fibrosis with mortality and sudden cardiac death in patients with nonischemic dilated cardiomyopathy. *JAMA*. 2013;309:896–908. doi: 10.1001/jama.2013.1363.
23. Iles L, Pfluger H, Lefkovits L, Butler MJ, Kistler PM, Kaye DM, Taylor AJ. Myocardial fibrosis predicts appropriate device therapy in patients with implantable cardioverter-defibrillators for primary prevention of sudden cardiac death. *J Am Coll Cardiol*. 2011;57:821–828. doi: 10.1016/j.jacc.2010.06.062.
24. Assomull RG, Prasad SK, Lyne J, Smith G, Burman ED, Khan M, Sheppard MN, Poole-Wilson PA, Pennell DJ. Cardiovascular magnetic resonance, fibrosis, and prognosis in dilated cardiomyopathy. *J Am Coll Cardiol*. 2006;48:1977–1985.
25. Chimura M, Kiuchi K, Okajima K, Shimane A, Sawada T, Onishi T, Yamada S, Taniguchi Y, Yasaka Y, Kawai H. Distribution of ventricular fibrosis associated with life threatening ventricular tachyarrhythmias in patients with nonishcemic dilated cardiomyopathy. *J Cardiovasc Electrophysiol*. 2015;26:1239–1246.
26. Wu KC, Weiss RG, Thiemann DR, Kitagawa K, Schmidt A, Dalal D, Lai S, Bluemke DA, Gerstenblith G, Marbán E, Tomaselli GF, Lima JA. Late gadolinium enhancement by cardiovascular magnetic resonance heralds an adverse prognosis in nonischemic cardiomyopathy. *J Am Coll Cardiol*. 2008;51:2414–2421. doi: 10.1016/j.jacc.2008.03.018.
27. Grün S, Schumm J, Greulich S, Wagner A, Schneider S, Bruder O, Kispert EM, Hill S, Ong P, Klingel K, Kandolf R, Sechtem U, Mahrholdt H. Long-term follow-up of biopsy-proven viral myocarditis: predictors of mortality and incomplete recovery. *J Am Coll Cardiol*. 2012;59:1604–1615. doi: 10.1016/j.jacc.2012.01.007.
28. Mehta D, Mori N, Goldbarg SH, Lubitz S, Wisnivesky JP, Teirstein A. Primary prevention of sudden cardiac death in silent cardiac sarcoidosis: role of programmed ventricular stimulation. *Circ Arrhythm Electrophysiol*. 2011;4:43–48. doi: 10.1161/CIRCEP.110.958322.
29. Bruder O, Wagner A, Jensen CJ, Schneider S, Ong P, Kispert EM, Nassenstein K, Schlosser T, Sabin GV, Sechtem U, Mahrholdt H. Myocardial scar visualized by cardiovascular magnetic resonance imaging predicts major adverse events in patients with hypertrophic cardiomyopathy. *J Am Coll Cardiol*. 2010;56:875–887. doi: 10.1016/j.jacc.2010.05.007.
30. Rubinshtein R, Glockner JF, Ommen SR, Araoz PA, Ackerman MJ, Sorajja P, Bos JM, Tajik AJ, Valeti US, Nishimura RA, Gersh BJ. Characteristics and clinical significance of late gadolinium enhancement by contrast-enhanced magnetic resonance imaging in patients with hypertrophic cardiomyopathy. *Circ Heart Fail*. 2010;3:51–58. doi: 10.1161/CIRCHEARTFAILURE.109.854026.
31. O'Hanlon R, Grasso A, Roughton M, Moon JC, Clark S, Wage R, Webb J, Kulkarni M, Dawson D, Sulaibeekh L, Chandrasekaran B, Bucciarelli-Ducci C, Pasquale F, Cowie MR, McKenna WJ, Sheppard MN, Elliott PM, Pennell DJ, Prasad SK. Prognostic significance of myocardial fibrosis in hypertrophic cardiomyopathy. *J Am Coll Cardiol*. 2010;56:867–874. doi: 10.1016/j.jacc.2010.05.010.
32. Scott PA, Morgan JM, Carroll N, Murday DC, Roberts PR, Peebles CR, Harden SP, Curzen NP. The extent of left ventricular scar quantified by late gadolinium enhancement MRI is associated with spontaneous ventricular arrhythmias in patients with coronary artery disease and implantable cardioverter-defibrillators. *Circ Arrhythm Electrophysiol*. 2011;4:324–330. doi: 10.1161/CIRCEP.110.959544.
33. Neilan TG, Coelho-Filho OR, Danik SB, Shah RV, Dodson JA, Verdini DJ, Tokuda M, Daly CA, Tedrow UB, Stevenson WG, Jerosch-Herold M, Ghoshhajra BB, Kwong RY. CMR quantification of myocardial scar provides additive prognostic information in nonischemic cardiomyopathy. *JACC Cardiovasc Imaging*. 2013;6:944–954. doi: 10.1016/j.jcmg.2013.05.013.
34. Bello D, Fieno DS, Kim RJ, Pereles FS, Passman R, Song G, Kadish AH, Goldberger JJ. Infarct morphology identifies patients with substrate for sustained ventricular tachycardia. *J Am Coll Cardiol*. 2005;45:1104–1108. doi: 10.1016/j.jacc.2004.12.057.
35. de Haan S, Meijers TA, Knaapen P, Beek AM, van Rossum AC, Allaart CP. Scar size and characteristics assessed by CMR predict ventricular arrhythmias in ischaemic cardiomyopathy: comparison of previously validated models. *Heart*. 2011;97:1951–1956. doi: 10.1136/heartjnl-2011-300060.
36. Klem I, Weinsaft JW, Bahnson TD, Hegland D, Kim HW, Hayes B, Parker MA, Judd RM, Kim RJ. Assessment of myocardial scarring improves risk stratification in patients evaluated for cardiac defibrillator implantation. *J Am Coll Cardiol*. 2012;60:408–420. doi: 10.1016/j.jacc.2012.02.070.
37. Yokokawa M, Tada H, Koyama K, Ino T, Hiramatsu S, Kaseno K, Naito S, Oshima S, Taniguchi K. The characteristics and distribution of the scar tissue predict ventricular tachycardia in patients with advanced heart failure. *Pacing Clin Electrophysiol*. 2009;32:314–322. doi: 10.1111/j.1540-8159.2008.02238.x.
38. Piers SR, Everaerts K, van der Geest RJ, Hazebroek MR, Siebelink HM, Pison LA, Schalij MJ, Bekkers SC, Heymans S, Zeppenfeld K. Myocardial scar predicts monomorphic ventricular tachycardia but not polymorphic ventricular tachycardia or ventricular fibrillation in nonischemic dilated cardiomyopathy. *Heart Rhythm*. 2015;12:2106–2114. doi: 10.1016/j.hrthm.2015.05.026.
39. Gao P, Yee R, Gula L, Krahn AD, Skanes A, Leong-Sit P, Klein GJ, Stirrat J, Fine N, Pallaveshi L, Wisenberg G, Thompson TR, Prato F, Drangova M, White JA. Prediction of arrhythmic events in ischemic and dilated cardiomyopathy patients referred for implantable cardiac defibrillator: evaluation of multiple scar quantification measures for late gadolinium enhancement magnetic resonance imaging. *Circ Cardiovasc Imaging*. 2012;5:448–456. doi: 10.1161/CIRCIMAGING.111.971549.
40. Fluechter S, Kuschyk J, Wolpert C, Doesch C, Veltmann C, Haghi D, Schoenberg SO, Sueselbeck T, Germans T, Streitner F, Borggrefe M, Pa-

pavassiliu T. Extent of late gadolinium enhancement detected by cardiovascular magnetic resonance correlates with the inducibility of ventricular tachyarrhythmia in hypertrophic cardiomyopathy. *J Cardiovasc Magn Reson*. 2010;12:30. doi: 10.1186/1532-429X-12-30.

41. Chan RH, Maron BJ, Olivotto I, Pencina MJ, Assenza GE, Haas T, Lesser JR, Gruner C, Crean AM, Rakowski H, Udelson JE, Rowin E, Lombardi M, Cecchi F, Tomberli B, Spirito P, Formisano F, Biagini E, Rapezzi C, De Cecco CN, Autore C, Cook EF, Hong SN, Gibson CM, Manning WJ, Appelbaum E, Maron MS. Prognostic value of quantitative contrast-enhanced cardiovascular magnetic resonance for the evaluation of sudden death risk in patients with hypertrophic cardiomyopathy. *Circulation*. 2014;130:484–495. doi: 10.1161/CIRCULATIONAHA.113.007094.
42. Yan AT, Shayne AJ, Brown KA, Gupta SN, Chan CW, Luu TM, Di Carli MF, Reynolds HG, Stevenson WG, Kwong RY. Characterization of the peri-infarct zone by contrast-enhanced cardiac magnetic resonance imaging is a powerful predictor of post-myocardial infarction mortality. *Circulation*. 2006;114:32–39. doi: 10.1161/CIRCULATIONAHA.106.613414.
43. Schmidt A, Azevedo CF, Cheng A, Gupta SN, Bluemke DA, Foo TK, Gerstenblith G, Weiss RG, Marbán E, Tomaselli GF, Lima JA, Wu KC. Infarct tissue heterogeneity by magnetic resonance imaging identifies enhanced cardiac arrhythmia susceptibility in patients with left ventricular dysfunction. *Circulation*. 2007;115:2006–2014. doi: 10.1161/CIRCULATIONAHA.106.653568.
44. Boyé P, Abdel-Aty H, Zacharzowsky U, Bohl S, Schwenke C, van der Geest RJ, Dietz R, Schirdewan A, Schulz-Menger J. Prediction of life-threatening arrhythmic events in patients with chronic myocardial infarction by contrast-enhanced CMR. *JACC Cardiovasc Imaging*. 2011;4:871–879. doi: 10.1016/j.jcmg.2011.04.014.
45. Roes SD, Borleffs CJ, van der Geest RJ, Westenberg JJ, Marsan NA, Kaandorp TA, Reiber JH, Zeppenfeld K, Lamb HJ, de Roos A, Schalij MJ, Bax JJ. Infarct tissue heterogeneity assessed with contrast-enhanced MRI predicts spontaneous ventricular arrhythmia in patients with ischemic cardiomyopathy and implantable cardioverter-defibrillator. *Circ Cardiovasc Imaging*. 2009;2:183–190. doi: 10.1161/CIRCIMAGING.108.826529.
46. Wu KC, Gerstenblith G, Guallar E, Marine JE, Dalal D, Cheng A, Marbán E, Lima JA, Tomaselli GF, Weiss RG. Combined cardiac magnetic resonance imaging and C-reactive protein levels identify a cohort at low risk for defibrillator firings and death. *Circ Cardiovasc Imaging*. 2012;5:178–186. doi: 10.1161/CIRCIMAGING.111.968024.
47. Lin LY, Su MY, Chen JJ, Lai LP, Hwang JJ, Tseng CD, Chen YS, Yu HY, Tseng WY, Lin JL. Conductive channels identified with contrast-enhanced MR imaging predict ventricular tachycardia in systolic heart failure. *JACC Cardiovasc Imaging*. 2013;6:1152–1159. doi: 10.1016/j.jcmg.2013.05.017.
48. Schelbert EB, Hsu LY, Anderson SA, Mohanty BD, Karim SM, Kellman P, Aletras AH, Arai AE. Late gadolinium-enhancement cardiac magnetic resonance identifies postinfarction myocardial fibrosis and the border zone at the near cellular level in ex vivo rat heart. *Circ Cardiovasc Imaging*. 2010;3:743–752. doi: 10.1161/CIRCIMAGING.108.835793.
49. Morishima I, Sone T, Tsuboi H, Mukawa H, Uesugi M, Morikawa S, Takagi K, Niwa T, Morita Y, Murakami R, Numaguchi Y, Murohara T, Okumura K. Risk stratification of patients with prior myocardial infarction and advanced left ventricular dysfunction by gated myocardial perfusion SPECT imaging. *J Nucl Cardiol*. 2008;15:631–637. doi: 10.1016/j.nuclcard.2008.03.009.
50. Verberne HJ, Brewster LM, Somsen GA, van Eck-Smit BL. Prognostic value of myocardial 123I-metaiodobenzylguanidine (MIBG) parameters in patients with heart failure: a systematic review. *Eur Heart J*. 2008;29:1147–1159. doi: 10.1093/eurheartj/ehn113.
51. Bax JJ, Kraft O, Buxton AE, Fjeld JG, Parízek P, Agostini D, Knuuti J, Flotats A, Arrighi J, Muxi A, Alibelli MJ, Banerjee G, Jacobson AF. 123 I-mIBG scintigraphy to predict inducibility of ventricular arrhythmias on cardiac electrophysiology testing: a prospective multicenter pilot study. *Circ Cardiovasc Imaging*. 2008;1:131–140. doi: 10.1161/CIRCIMAGING.108.782433.
52. Bogun FM, Desjardins B, Good E, Gupta S, Crawford T, Oral H, Ebinger M, Pelosi F, Chugh A, Jongnarangsin K, Morady F. Delayed-enhanced magnetic resonance imaging in nonischemic cardiomyopathy: utility for identifying the ventricular arrhythmia substrate. *J Am Coll Cardiol*. 2009;53:1138–1145. doi: 10.1016/j.jacc.2008.11.052.
53. Kumar S, Tedrow UB, Stevenson WG. Adjunctive interventional techniques when percutaneous catheter ablation for drug refractory ventricular arrhythmias fail: a contemporary review. *Circ Arrhythm Electrophysiol*. 2017;10:e003676. doi: 10.1161/CIRCEP.116.003676.
54. Sosa E, Scanavacca M, d'Avila A, Pilleggi F. A new technique to perform epicardial mapping in the electrophysiology laboratory. *J Cardiovasc Electrophysiol*. 1996;7:531–536.
55. Kojima S, Yamada N, Goto Y. Diagnosis of constrictive pericarditis by tagged cine magnetic resonance imaging. *N Engl J Med*. 1999;341:373–374. doi: 10.1056/NEJM199907293410515.
56. Bogaert J, Francone M. Pericardial disease: value of CT and MR imaging. *Radiology*. 2013;267:340–356. doi: 10.1148/radiol.13121059.
57. Weinsaft JW, Kim HW, Shah DJ, Klem I, Crowley AL, Brosnan R, James OG, Patel MR, Heitner J, Parker M, Velazquez EJ, Steenbergen C, Judd RM, Kim RJ. Detection of left ventricular thrombus by delayed-enhancement cardiovascular magnetic resonance prevalence and markers in patients with systolic dysfunction. *J Am Coll Cardiol*. 2008;52:148–157. doi: 10.1016/j.jacc.2008.03.041.
58. Weinsaft JW, Kim RJ, Ross M, Krauser D, Manoushagian S, LaBounty TM, Cham MD, Min JK, Healy K, Wang Y, Parker M, Roman MJ, Devereux RB. Contrast-enhanced anatomic imaging as compared to contrast-enhanced tissue characterization for detection of left ventricular thrombus. *JACC Cardiovasc Imaging*. 2009;2:969–979. doi: 10.1016/j.jcmg.2009.03.017.
59. Aliot EM, Stevenson WG, Almendral-Garrote JM, Bogun F, Calkins CH, Delacretaz E, Della Bella P, Hindricks G, Jaïs P, Josephson ME, Kautzner J, Kay GN, Kuck KH, Lerman BB, Marchlinski F, Reddy V, Schalij MJ, Schilling R, Soejima K, Wilber D; European Heart Rhythm Association (EHRA); Registered Branch of the European Society of Cardiology (ESC); Heart Rhythm Society (HRS); American College of Cardiology (ACC); American Heart Association (AHA). EHRA/HRS expert consensus on catheter ablation of ventricular arrhythmias: developed in a partnership with the European Heart Rhythm Association (EHRA), a registered branch of the European Society of Cardiology (ESC), and the Heart Rhythm Society (HRS); in collaboration with the American College of Cardiology (ACC) and the American Heart Association (AHA). *Heart Rhythm*. 2009;6:886–933. doi: 10.1016/j.hrthm.2009.04.030.
60. Berte B, Yamashita S, Sacher F, Cochet H, Hooks D, Aljefairi N, Amraoui S, Denis A, Derval N, Hocini M, Haïssaguerre M, Jaïs P. Epicardial only mapping and ablation of ventricular tachycardia: a case series. *Europace*. 2016;18:267–273. doi: 10.1093/europace/euv072.
61. Codreanu A, Odille F, Aliot E, Marie PY, Magnin-Poull I, Andronache M, Mandry D, Djaballah W, Régent D, Felblinger J, de Chillou C. Electroanatomic characterization of post-infarct scars comparison with 3-dimensional myocardial scar reconstruction based on magnetic resonance imaging. *J Am Coll Cardiol*. 2008;52:839–842. doi: 10.1016/j.jacc.2008.05.038.
62. Wijnmaalen AP, van der Geest RJ, van Huls van Taxis CF, Siebelink HM, Kroft LJ, Bax JJ, Reiber JH, Schalij MJ, Zeppenfeld K. Head-to-head comparison of contrast-enhanced magnetic resonance imaging and electroanatomical voltage mapping to assess post-infarct scar characteristics in patients with ventricular tachycardias: real-time image integration and reversed registration. *Eur Heart J*. 2011;32:104–114. doi: 10.1093/eurheartj/ehq345.
63. Fernández-Armenta J, Berruezo A, Andreu D, Camara O, Silva E, Serra L, Barbarito V, Carotenutto L, Evertz R, Ortiz-Pérez JT, De Caralt TM, Perea RJ, Sitges M, Mont L, Frangi A, Brugada J. Three-dimensional architecture of scar and conducting channels based on high resolution ce-CMR: insights for ventricular tachycardia ablation. *Circ Arrhythm Electrophysiol*. 2013;6:528–537. doi: 10.1161/CIRCEP.113.000264.
64. Marra MP, Leoni L, Bauce B, Corbetti F, Zorzi A, Migliore F, Silvano M, Rigato I, Tona F, Tarantini G, Cacciavillani L, Basso C, Buja G, Thiene G, Iliceto S, Corrado D. Imaging study of ventricular scar in arrhythmogenic right ventricular cardiomyopathy: comparison of 3D standard electroanatomical voltage mapping and contrast-enhanced cardiac magnetic resonance. *Circ Arrhythm Electrophysiol*. 2012;5:91–100. doi: 10.1161/CIRCEP.111.964635.
65. Yamashita S, Sacher F, Mahida S, Berte B, Lim HS, Komatsu Y, Amraoui S, Denis A, Derval N, Laurent F, Montaudon M, Hocini M, Haïssaguerre M, Jaïs P, Cochet H. Role of high-resolution image integration to visualize left phrenic nerve and coronary arteries during epicardial ventricular tachycardia ablation. *Circ Arrhythm Electrophysiol*. 2015;8:371–380. doi: 10.1161/CIRCEP.114.002420.
66. Desjardins B, Crawford T, Good E, Oral H, Chugh A, Pelosi F, Morady F, Bogun F. Infarct architecture and characteristics on delayed enhanced magnetic resonance imaging and electroanatomic mapping in patients with postinfarction ventricular arrhythmia. *Heart Rhythm*. 2009;6:644–651. doi: 10.1016/j.hrthm.2009.02.018.

67. Gupta S, Desjardins B, Baman T, Ilg K, Good E, Crawford T, Oral H, Pelosi F, Chugh A, Morady F, Bogun F. Delayed-enhanced MR scar imaging and intraprocedural registration into an electroanatomical mapping system in post-infarction patients. *JACC Cardiovasc Imaging*. 2012;5:207–210. doi: 10.1016/j.jcmg.2011.08.021.
68. Andreu D, Ortiz-Pérez JT, Boussy T, Fernández-Armenta J, de Caralt TM, Perea RJ, Prat-González S, Mont L, Brugada J, Berruezo A. Usefulness of contrast-enhanced cardiac magnetic resonance in identifying the ventricular arrhythmia substrate and the approach needed for ablation. *Eur Heart J*. 2014;35:1316–1326. doi: 10.1093/eurheartj/eht510.
69. Andreu D, Berruezo A, Ortiz-Pérez JT, Silva E, Mont L, Borràs R, de Caralt TM, Perea RJ, Fernández-Armenta J, Zeljko H, Brugada J. Integration of 3D electroanatomic maps and magnetic resonance scar characterization into the navigation system to guide ventricular tachycardia ablation. *Circ Arrhythm Electrophysiol*. 2011;4:674–683. doi: 10.1161/CIRCEP.111.961946.
70. Sasaki T, Miller CF, Hansford R, Yang J, Caffo BS, Zviman MM, Henrikson CA, Marine JE, Spragg D, Cheng A, Tandri H, Sinha S, Kolandaivelu A, Zimmerman SL, Bluemke DA, Tomaselli GF, Berger RD, Calkins H, Halperin HR, Nazarian S. Myocardial structural associations with local electrograms: a study of postinfarct ventricular tachycardia pathophysiology and magnetic resonance-based noninvasive mapping. *Circ Arrhythm Electrophysiol*. 2012;5:1081–1090. doi: 10.1161/CIRCEP.112.970699.
71. Dickfeld T, Tian J, Ahmad G, Jimenez A, Turgeman A, Kuk R, Peters M, Saliaris A, Saba M, Shorofsky S, Jeudy J. MRI-guided ventricular tachycardia ablation: integration of late gadolinium-enhanced 3D scar in patients with implantable cardioverter-defibrillators. *Circ Arrhythm Electrophysiol*. 2011;4:172–184. doi: 10.1161/CIRCEP.110.958744.
72. Piers SR, Tao Q, de Riva Silva M, Siebelink HM, Schalij MJ, van der Geest RJ, Zeppenfeld K. CMR-based identification of critical isthmus sites of ischemic and nonischemic ventricular tachycardia. *JACC Cardiovasc Imaging*. 2014;7:774–784. doi: 10.1016/j.jcmg.2014.03.013.
73. Yamashita S, Sacher F, Mahida S, Berte B, Lim HS, Komatsu Y, Amraoui S, Denis A, Derval N, Laurent F, Sermesant M, Montaudon M, Hocini M, Haïssaguerre M, Jaïs P, Cochet H. Image integration to guide catheter ablation in scar-related ventricular tachycardia. *J Cardiovasc Electrophysiol*. 2016;27:699–708. doi: 10.1111/jce.12963.
74. Desjardins B, Morady F, Bogun F. Effect of epicardial fat on electroanatomical mapping and epicardial catheter ablation. *J Am Coll Cardiol*. 2010;56:1320–1327. doi: 10.1016/j.jacc.2010.04.054.
75. Dickfeld T, Lei P, Dilsizian V, Jeudy J, Dong J, Voudouris A, Peters R, Saba M, Shekhar R, Shorofsky S. Integration of three-dimensional scar maps for ventricular tachycardia ablation with positron emission tomography-computed tomography. *JACC Cardiovasc Imaging*. 2008;1:73–82. doi: 10.1016/j.jcmg.2007.10.001.
76. Tian J, Smith MF, Chinnadurai P, Dilsizian V, Turgeman A, Abbo A, Gajera K, Xu C, Plotnick D, Peters R, Saba M, Shorofsky S, Dickfeld T. Clinical application of PET/CT fusion imaging for three-dimensional myocardial scar and left ventricular anatomy during ventricular tachycardia ablation. *J Cardiovasc Electrophysiol*. 2009;20:567–604. doi: 10.1111/j.1540-8167.2008.01377.x.
77. Fahmy TS, Wazni OM, Jaber WA, Walimbe V, Di Biase L, Elayi CS, DiFilippo FP, Young RB, Patel D, Riedlbauchova L, Corrado A, Burkhardt JD, Schweikert RA, Arruda M, Natale A. Integration of positron emission tomography/computed tomography with electroanatomical mapping: a novel approach for ablation of scar-related ventricular tachycardia. *Heart Rhythm*. 2008;5:1538–1545. doi: 10.1016/j.hrthm.2008.08.020.
78. Klein T, Abdulghani M, Smith M, Huang R, Asoglu R, Remo BF, Turgeman A, Mesubi O, Sidhu S, Synowski S, Saliaris A, See V, Shorofsky S, Chen W, Dilsizian V, Dickfeld T. Three-dimensional 123I-meta-iodobenzylguanidine cardiac innervation maps to assess substrate and successful ablation sites for ventricular tachycardia: feasibility study for a novel paradigm of innervation imaging. *Circ Arrhythm Electrophysiol*. 2015;8:583–591. doi: 10.1161/CIRCEP.114.002105.
79. Tian J, Smith MF, Ahmad G, Dilsizian V, Jimenez A, Dickfeld T. Integration of 3-dimensional scar models from SPECT to guide ventricular tachycardia ablation. *J Nucl Med*. 2012;53:894–901. doi: 10.2967/jnumed.111.094904.
80. Bala R, Ren JF, Hutchinson MD, Desjardins B, Tschabrunn C, Gerstenfeld EP, Deo R, Dixit S, Garcia FC, Cooper J, Lin D, Riley MP, Tzou WS, Verdino R, Epstein AE, Callans DJ, Marchlinski FE. Assessing epicardial substrate using intracardiac echocardiography during VT ablation. *Circ Arrhythm Electrophysiol*. 2011;4:667–673. doi: 10.1161/CIRCEP.111.963553.
81. Bunch TJ, Weiss JP, Crandall BG, Day JD, DiMarco JP, Ferguson JD, Mason PK, McDaniel G, Osborn JS, Wiggins D, Mahapatra S. Image integration using intracardiac ultrasound and 3D reconstruction for scar mapping and ablation of ventricular tachycardia. *J Cardiovasc Electrophysiol*. 2010;21:678–684. doi: 10.1111/j.1540-8167.2009.01680.x.
82. Khaykin Y, Skanes A, Whaley B, Hill C, Beardsall M, Seabrook C, Wulffhart Z, Oosthuizen R, Gula L, Verma A. Real-time integration of 2D intracardiac echocardiography and 3D electroanatomical mapping to guide ventricular tachycardia ablation. *Heart Rhythm*. 2008;5:1396–1402. doi: 10.1016/j.hrthm.2008.06.025.
83. Dickfeld T, Kato R, Zviman M, Lai S, Meininger G, Lardo AC, Roguin A, Blumke D, Berger R, Calkins H, Halperin H. Characterization of radiofrequency ablation lesions with gadolinium-enhanced cardiovascular magnetic resonance imaging. *J Am Coll Cardiol*. 2006;47:370–378. doi: 10.1016/j.jacc.2005.07.070.
84. Berte B, Sacher F, Mahida S, Yamashita S, Lim HS, Denis A, Derval N, Hocini M, Haïssaguerre M, Cochet H, Jaïs P. Impact of septal radiofrequency ventricular tachycardia ablation: insights from magnetic resonance imaging. *Circulation*. 2014;130:716–718. doi: 10.1161/CIRCULATIONAHA.114.010175.
85. Ilg K, Baman TS, Gupta SK, Swanson S, Good E, Chugh A, Jongnarangsin K, Pelosi F Jr, Crawford T, Oral H, Morady F, Bogun F. Assessment of radiofrequency ablation lesions by CMR imaging after ablation of idiopathic ventricular arrhythmias. *JACC Cardiovasc Imaging*. 2010;3:278–285. doi: 10.1016/j.jcmg.2009.09.028.
86. Abdulghani M, Duell J, Smith M, Chen W, Bentzen SM, Asoglu R, Klein T, Bob-Manuel T, Saliaris A, See V, Shorofsky S, Dilsizian V, Dickfeld T. Global and regional myocardial innervation before and after ablation of drug-refractory ventricular tachycardia assessed with 123I-MIBG. *J Nucl Med*. 2015;56(suppl 4):52S–58S. doi: 10.2967/jnumed.115.155143.
87. Vergara GR, Vijayakumar S, Kholmovski EG, Blauer JJ, Guttman MA, Gloschat C, Payne G, Vij K, Akoum NW, Daccarett M, McGann CJ, Macleod RS, Marrouche NF. Real-time magnetic resonance imaging-guided radiofrequency atrial ablation and visualization of lesion formation at 3 Tesla. *Heart Rhythm*. 2011;8:295–303. doi: 10.1016/j.hrthm.2010.10.032.
88. Bisbal F, Fernández-Armenta J, Berruezo A, Mont L, Brugada J. Use of MRI to guide electrophysiology procedures. *Heart*. 2014;100:1975–1984. doi: 10.1136/heartjnl-2013-304692.
89. Oster HS, Taccardi B, Lux RL, Ershler PR, Rudy Y. Noninvasive electrocardiographic imaging: reconstruction of epicardial potentials, electrograms, and isochrones and localization of single and multiple electrocardiac events. *Circulation*. 1997;96:1012–1024.
90. Burnes JE, Taccardi B, Rudy Y. A noninvasive imaging modality for cardiac arrhythmias. *Circulation*. 2000;102:2152–2158.
91. Wang Y, Cuculich PS, Zhang J, Desouza KA, Vijayakumar R, Chen J, Faddis MN, Lindsay BD, Smith TW, Rudy Y. Noninvasive electroanatomic mapping of human ventricular arrhythmias with electrocardiographic imaging. *Sci Transl Med*. 2011;3:98ra84. doi: 10.1126/scitranslmed.3002152.
92. Arevalo HJ, Vadakkumpadan F, Guallar E, Jebb A, Malamas P, Wu KC, Trayanova NA. Arrhythmia risk stratification of patients after myocardial infarction using personalized heart models. *Nat Commun*. 2016;7:11437. doi: 10.1038/ncomms11437.
93. Cedilnik N, Duchateau J, Dubois R, Jaïs P, Cochet H, Sermesant M. (2017) VT Scan: Towards an Efficient Pipeline from Computed Tomography Images to Ventricular Tachycardia Ablation. In: Pop M, Wright G (eds). *Functional Imaging and Modelling of the Heart*. FIMH 2017. Lecture Notes in Computer Science. Toronto, Canada: Springer; 2017, vol 10263.
94. Ashikaga H, Sasano T, Dong J, Zviman MM, Evers R, Hopenfeld B, Castro V, Helm RH, Dickfeld T, Nazarian S, Donahue JK, Berger RD, Calkins H, Abraham MR, Marbán E, Lardo AC, McVeigh ER, Halperin HR. Magnetic resonance-based anatomical analysis of scar-related ventricular tachycardia: implications for catheter ablation. *Circ Res*. 2007;101:939–947. doi: 10.1161/CIRCRESAHA.107.158980.
95. Andreu D, Ortiz-Pérez JT, Fernández-Armenta J, Guiu E, Acosta J, Prat-González S, De Caralt TM, Perea RJ, Garrido C, Mont L, Brugada J, Berruezo A. 3D delayed-enhanced magnetic resonance sequences improve conducting channel delineation prior to ventricular tachycardia ablation. *Europace*. 2015;17:938–945. doi: 10.1093/europace/euu310.
96. Perez-David E, Arenal A, Rubio-Guivernau JL, del Castillo R, Atea L, Arbelo E, Caballero E, Celorrio V, Datino T, Gonzalez-Torrecilla E, Atienza F, Ledesma-Carbayo MJ, Bermejo J, Medina A, Fernández-Avilés F. Noninvasive

identification of ventricular tachycardia-related conducting channels using contrast-enhanced magnetic resonance imaging in patients with chronic myocardial infarction: comparison of signal intensity scar mapping and endocardial voltage mapping. *J Am Coll Cardiol*. 2011;57:184–194. doi: 10.1016/j.jacc.2010.07.043.

97. Helm PA, Caravan P, French BA, Jacques V, Shen L, Xu Y, Beyers RJ, Roy RJ, Kramer CM, Epstein FH. Postinfarction myocardial scarring in mice: molecular MR imaging with use of a collagen-targeting contrast agent. *Radiology*. 2008;247:788–796. doi: 10.1148/radiol.2473070975.
98. Cochet H, Dubois R, Sacher F, Derval N, Sermesant M, Hocini M, Montaudon M, Haïssaguerre M, Laurent F, Jaïs P. Cardiac arrythmias: multimodal assessment integrating body surface ECG mapping into cardiac imaging. *Radiology*. 2014;271:239–247. doi: 10.1148/radiol.13131331.

Circulation

Cardiac Imaging in Patients With Ventricular Tachycardia

Saagar Mahida, Frédéric Sacher, Rémi Dubois, Maxime Sermesant, Frank Bogun, Michel Haïssaguerre, Pierre Jaïs and Hubert Cochet

Circulation. 2017;136:2491-2507
doi: 10.1161/CIRCULATIONAHA.117.029349
Circulation is published by the American Heart Association, 7272 Greenville Avenue, Dallas, TX 75231

Print ISSN: 0009-7322. Online ISSN: 1524-4539

Supplemental Material

Cardiac Imaging in Patients with Ventricular Tachycardia

Saagar Mahida, MD, PhD[1], Frédéric Sacher, MD, PhD[2], Rémi Dubois, PhD[2], Maxime Sermesant, PhD[3], Frank Bogun, MD[4], Michel Haïssaguerre, MD[2], Pierre Jaïs, MD[2], and Hubert Cochet, MD, PhD.[2]

1 Liverpool Heart and Chest Hospital, Liverpool, United Kingdom
2 LIRYC Institute, CHU Bordeaux/University of Bordeaux, Bordeaux, France
3 Inria Sophia Antipolis, Sophia Antipolis - Méditerranée, France
4 University of Michigan, Ann Arbor, MI, USA

Supplemental table 1. Summary of studies investigating the role of LGE-CMR in risk prediction

Cardiomyopathy	No. of patients	Previous arrhythmias	Scar definition	Risk	Outcome	Ref
Multiple cardiomyopathies	373	Sustained VT and NSVT		Cardiac death, SCD, ICD shock (sustained VT); Presence of fibrosis (HR per segment, 3.3; 95 CI, 1.8 - 5.8; P=0.001)	CMR-detected fibrosis is an independent predictor of recurrent ventricular arrhythmia	[1]
ICM	144	No	Relative to remote normal myocardium Core; SI >3 SDs Border zone; SI 2 - 3 SDs	All-cause mortality (HR, 1.42; P=0.005) and cardiovascular mortality (HR, 1.49; P=0.01)	Extent of peri-infarct zone predictor of cardiovascular and all cause mortality	[2]
ICM	64	No	Scar: ≥50% of MSI	ICD shock: % scar (HR per 10%, 1.75; 95% CI, 1.09 to 2.81; P=0.02) ICD shock: Number of transmural scar segments (HR per segment, 1.40; 95 CI, 1.15 to 1.70; P=0.001)	Scar extent associated with occurrence of spontaneous ventricular arrhythmias	[3]
ICM	47	No	Core: ≥50% of MSI Borderzone: SI>peak remote SI but <50% MSI	Scar heterogeneity associated with VT inducibility (p=0.015) Total scar not associated with VT inducibility (p=0.17) Scar core not associated with VT inducibility (p=0.95)	Scar heterogeneity is associated with VT inducibility	[4]
NICM	472	No		SCD; fibrosis presence: HR, 4.61 [95% CI, 2.75-7.74], P < 0.001; and by fibrosis extent: HR, 1.10 [95% CI, 1.05-1.16], P < 0.001),	Presence and extent of scar associated with SCD and all-cause mortality	[5]
NICM	162	No		LGE extent predicts cardiovascular death and appropriate ICD therapy HR: 7.61; p < 0.0001 per 10%	Scar extent predicts cardiovascular death and appropriate ICD therapy	[6]
NICM	61	No		ICD discharges NICM with LGE 14%, vs. NICM without LGE 0% (p < 0.01)	Presence of LGE predicts ICD therapy while absence of LGE is associated with a favorable prognosis	[7]
NICM	101	No		SCD/VT; midwall fibrosis; HR 5.9; 95% CI 1.1 to 32.2; p = 0.04)	Midwall fibrosis is predictive of SCD/VT as well as all-cause mortality	[8]

ICM	48	No		Infarct surface area as predictor of inducible VT; X_2 6.6 and p<0.01 Infarct mass as predictor of inducible VT; chi-square and p values 4.5 and <0.03	CMR infarct mass and surface area predict inducibility of VT during programmed stimulation	[9]
ICM	52	No		Relative infarct transmurality independent predictor of ICD therapy or cardiovascular death (p = 0.02)	Infarct transmurality predicts life-threatening arrhythmias and cardiac death.	[10]
ICM	46	No	Scar SI< 2 SD above remote normal myocardium	Patients with VT inducibility had more infarcted (*P* <0.01) and border zone (*P*< 0.01) sectors Peak circumferential shortening strain was greater in patients with inducible VT (<0.05)	Enhanced border zone function is correlated with inducibility of monomorphic VT in ICM patients	[11]
ICM	91	No	Core: ≥50% of MSI Border zone: 35% to 50% of MSI	Infarct gray zone predicts spontaneous ventricular arrhythmia and ICD therapy (HR, 1.49/10 g; CI, 1.01 to 2.20; chi (2)=4.0; P=0.04)	CMR-defined infarct heterogeneity is a strong predictor of spontaneous ventricular arrhythmia and ICD therapy	[12]
ICM	55	No	Core: ≥50% of MSI; Border zone: 35% to 50% of MSI Relative to remote normal myocardium Core; SI >3 SDs; Border zone; SI 2 - 3 SDs Core: ≥50% of MSI; Borderzone: SI>peak remote SI but <50% MSI	Total scar larger in patients with VT p=<0.001 – 0.008; AUC 0.75-0.79 Scar core larger in patients with VT p=<0.001 – 0.002; AUC 0.72-0.79 Scar border zone larger in patients with VT p=0.006 – 0.052; AUC 0.78-0.81	Total scar size, scar core size and peri-infarct zone size associated with increased risk of ventricular arrhythmia. Each parameter associated with comparable predictive value. Different methodologies for scar prediction associated with comparable predictive value	[13]
ICM	18	No	Scar >6 SD above remote normal myocardium	Scar volume smaller in VT patients (P < 0.0001)	Scar volume and number of scar segments not associated with VT	[14]

				No. of segments with scar smaller in VT patients (P < 0.005)		
ICM and NICM	137	No		SCD or ICD discharge; scar size > 5% of LV mass HR 4.76 (CI 1.65-13.7, p=0.004)	CMR-defined scar size is an independent predictor of adverse outcome (SCD, ICD discharges and overall mortality	15
ICM and NICM	235	No	Core: ≥50% of MSI; Borderzone: SI>peak remote SI but <50% MSI	ICD shock; More extensive scar gray zone; HR 4.6 (CI 1.4–15.4)	Extent of scar gray zone associated with ICD discharges and cardiac death	16
NICM	29	No	Scar >6 SD above remote normal myocardium	Scar volume larger in VT patients (P < 0.01) No. of segments with scar larger in VT patients (P < 0.0001)	Scar volume and number of scar segments associated with VT	14
NICM	87	No	Core: ≥50% of MSI Border zone: 35% to 50% of MSI	Monomorphic VT; Core, per 10 g↑; 4.28 (2.15–8.51) Monomorphic VT; Gray zone, per 10 g↑; 2.59 (1.38–4.86)	Extent of CMR-defined scar predicts monomorphic (optimal cutoff value to predict VT 7.2 g). Greater extent of scar in basal segments associated with higher risk.	17
NICM	175	No		SCD, VT or VF; septal and lateral mid-wall scar; HR 23.1 CI; 2.88-184.9, p = 0.003) No arrhythmias in absence of LGE	The absence of scar predicts a low risk of SCD and ventricular arrhythmia Presence of LGE had a high sensitivity but only a modest specificity in predicting life-threatening arrhythmic events	18
ICM and NICM	63	No	Relative to remote normal myocardium Core; SI >3 SDs Border zone; SI 2 - 3 SDs	VT/VF episodes; presence of conducting channels predictive; (HR: 27.03, 95% confidence interval [CI]: 3.29 - 222.05, p = 0.002) VT/VF episodes; % scar core not predictive; HR 3.75 (CI 0.753–18.677) p = 0.106	Presence of conducting channels predictive of VT/VF events Extent of scar core or scar border zone not predictive of VT/VF events	19

				VT/VF episodes; scar gray zone not predictive; 0.25 (0.05–1.25) p = 0.091		
NICM	26	No	Scar: >6 SD above remote normal myocardium	Scar transmurality (26% to 75%); ventricular arrhythmia inducibility (OR, 9.125; *P*=0.020)	Scar transmurality predicts VT inducibility	[1]
ICM and NICM	124	No	Relative to remote normal myocardium Core; SI >3 SDs Border zone; SI 2 - 3 SDs	SCD, ICD therapy; ICM; scar extent predictive; ≥2SD per 10g; HR 1.70 (CI 1.26–2.30, p=0.001) SCD, ICD therapy; NICM; scar extent predictive; ≥2SD per 10g; HR 1.31 (CI 1.08–1.60, p=0.007) SCD, ICD therapy; ICM; scar gray zone not predictive; HR 2.04 (CI 0.60–6.88)	Scar quantification predicts arrhythmic events in NICM and ICM	[20]
NICM	65	No		HF hospitalization, ICD therapy, and cardiac death; presence LGE-CMR of LGE; HR 8.2 (95% CI 2.2 to 30.9; p = 0.002)	Presence of scar strongly predicts adverse cardiac outcomes	[21]
Viral myocarditis	203	No		Presence of LGE associated with cardiac mortality (HR: 12.8, p < 0.01) No patient without LGE experienced SCD	Presence of scar strong predictor of cardiac mortality	[22]
Sarcoidosis	81	No		Presence of LGE associated with an 11.5-fold higher risk of cardiac death	Presence of scar predictor of cardiac mortality	[23]
HCM	76	No		% of LV mass with LGE; patients with inducible ventricular arrhythmias vs. those without; 22% versus 10%, p = 0.03	Extent of scar predictor of ventricular arrhythmias	[24]
HCM	1293	No		Extent of LGE associated with increased SCD risk (HR, 1.46/10% increase in LGE; *P*=0.002)	Extent of scar predictor of SCD	[25]
HCM	243	No		Presence of LGE; OR 5.47 for all-cause mortality; OR 8.01 for cardiac mortality	Scar is a good independent predictor of all-cause and cardiac mortality	[26]
HCM	424	No		SCD/ICD shock more frequent in LGE positive patients (LGE positive vs. LGE negative p = 0.01)	Scar strongly associated with arrhythmic events	[27]

HCM	217	No		Combined end point of cardiovascular death, cardiovascular admission, VT/VF, ICD shock; HR 3.4, p = 0.006	Scar an independent predictor of prognosis	[28]

Abbreviations: ICM, ischemic cardiomyopathy; HR, hazard ratio; LGE, late Gadolinium enhancement; LV, left ventricle; MSI, maximum signal intensity; OR, odds ratio; SCD, sudden cardiac death; SI, signal intensity; SD, standard deviation, SPECT, technetium 99m-tetrofosmin single photon emission computed tomography; VT ventricular tachycardia;

Supplemental table 2. Summary of studies comparing non-invasive imaging-defined scar and EAM-defined arrhythmogenic substrate

Modality	Cardiomyopathy		Scar definition	Result	Outcome	Ref
LGE-CMR	ICM	10		1.5 mV cutoff; MRI infarct surfaces correlation to EAM scar areas (r^2 = 0.82, p < 0.0001) Optimal cutoff values to differentiate scar from non-scar defined by MRI: Bipolar; 1.54 mV (AUC, 0.85); Unipolar; 6.52 mV (AUC: 0.87) Mismatch >20% in infarct surface measurement 33% scar areas	Significant mismatch between EAM-scar and LGE-CMR scar	[29]
LGE-CMR	ICM	14	Relative to remote normal myocardium Core; SI >3 SDs Border zone; SI 2 - 3 SDs	1.5 mV cutoff; MRI infarct surfaces correlation to EAM; 26% false positive, 3% false negative, 29% error Optimal cutoff values to differentiate scar from non-scar defined by MRI: Bipolar; 1.3 mV (13% false-positive, 5% false-negative, for a total error of 18%); Unipolar; 5.5 mV (9% false-positive, 7% false-negative, for a total error of 16%) All VT isthmuses located within LGE-CMR scar	Good correlation between EAM- and LGE-CMR scar and VT isthmuses and LGE-CMR scar	[30]
LGE-CMR	NICM	29		1.5 mV cutoff; Endocardial MRI scar correlation to EAM (R=0.94, p<0.0001) 87% of low voltage electrograms located in scar All VT isthmuses located within LGE-CMR scar	Good correlation between EAM- and LGE-CMR scar and VT isthmuses and LGE-CMR scar	[31]
LGE-CMR	ICM	15	Core: ≥50% of MSI Border zone: 35% to 50% of MSI	1.5 mV cutoff; correlation EAM- to LGE-CMR scar >25% transmurality (R=0.91). Mismatch between LGE-CMR and EAM scar in 33% patients (LGE-CMR scar > EAM scar) Subendocardial to transmural core infarct; median bipolar voltages; 2.2 (1.1 – 2.5), 1.5 (0.9 – 2.2), 1.1 (0.6–1.7), and 0.8 (0.4–1.3) mV for 25%, 50%, 75%, and 100% scar transmurality. Subendocardial to transmural grey zones, median bipolar voltages; 2.2 (1.3–3.3), 1.7 (0.8–2.4), 1.5 (0.7–2.5), and 1.0 (0.6–2.1) mV for 25%, 50%, 75%, and 100% scar transmurality	A cut-off value of 1.5 mV cannot fully delineate non-transmural scar, small subepicardial scar, and infarct gray-zones as identified by LGE-CMR. Bipolar voltage decreased with increasing scar transmurality Areas not detected by EAM non-transmural on LGE-CMR	[32]

LGE-CMR	ICM and NICM	14		1.5 mV cutoff; 75% correlation between LGE-CMR- and EAM-defined scar Optimal cutoff values to differentiate endocardial scar from non-scar defined by MRI: Bipolar; 1.49 mV (AUC, 0.86 0.01) Unipolar; 4.46 mV (AUC, 0.78 0.02) Bipolar voltage decreased with increasing scar transmurality ($R=0.83$, $P < 0.01$) 100% successful ablation sites located within scar – 76% in scar periphery Abnormal electrograms more frequently located in proximity to the scar border zone and in regions with greater (>50%) scar transmurality	Good correlation between EAM- and LGE-CMR scar and VT isthmuses and LGE-CMR scar	[33]
LGE-CMR	ICM	21	Core: 60% of MSI Border zone: 40% MSI	1.5 mV cutoff; moderate correlation between EAM endocardial scar and LGE-CMR total endocardial scar ($\rho=0.57$; $P<0.01$). 0.5 mV cutoff; EAM endocardial scar correlation to LGE-CMR dense endocardial scar moderate correlation ($\rho=0.58$; $p <0.01$) 1.5 mV cutoff; EAM epicardial scar correlation to LGE-CMR total epicardial scar; no significant correlation ($\rho=0.80$; $p=0.20$) LGE-CMR border zone channels identified 74% of critical isthmuses and 50% conducting channels identified by EAM	Moderate correlation between EAM- and LGE-CMR scar Good correlation between LGE-CMR- and EAM-defined conducting channels/VT isthmuses	[34]
LGE-CMR	ARVC	23		Low concordance between EAM and LGE-CMR ($\kappa=0.026$).	LGE-CMR is less sensitive than EAM in identifying right ventricular scar	[35]
LGE-CMR	ICM	18	Relative to remote normal myocardium Core; SI >3 SDs Border zone; SI 2 - 3 SDs	1.5 mV cutoff; EAM total endocardial scar correlation to LGE-CMR (<2 SD); ($r^2=0.4$, $p<0.009$) 0.5 mV cutoff; No significant correlation between EAM scar core and LGE-CMR scar core (<3 SD) Heterogeneous channels within scar coincided in location and orientation with a corresponding conducting channels in the voltage maps	Good correlation between EAM- and LGE-CMR scar and between LGE-CMR- and EAM-defined conducting channels	[36]

LGE-CMR	ICM	10		LGE-CMR MSI 60% to discriminate between core and BZ: Scar core (0.5 mV cutoff) - r^2=0.827, p=0.001; scar border zone (>0.5 - <1.5 mV) - (r^2=0.511, p=0.020) LGE-CMR MSI 50% to discriminate between core and BZ: Scar core (0.5 mV cutoff); (r^2=0.811, p=0.001) Scar border zone (>0.5 - <1.5 mV); MSI 60%; (r^2=0.594, p=0.009) 69% of conducting channels identified on EAM were identified on LGE-CMR	Good correlation between EAM- and LGE-CMR scar (MSI of 60% superior for discrimination between core and BZ) Good correlation between LGE-CMR- and EAM-defined conducting channels	37
LGE-CMR	ICM, NICM, ARVC	35	Core: ≥50% of MSI Border zone: 35% - 50% of MSI	1.5 mV cutoff; agreement between epicardial LGE-CMR- and EAM-defined substrate higher in ICM as compared to NICM (ICM 73±7% vs. NICM 32±12%, p=0.009) ICM: 92% LAVA located within LGE-CMR scar NICM: 88% LAVA located within LGE-CMR scar	Correlation between LGE-CMR- and EAM-defined substrate lower in NICM as compared to ICM	38
LGE-CMR	ICM	23	2 SDs above remote normal myocardium	1.5 mV cutoff; correlation EAM- to LGE-CMR scar R=0.62; p=0.003 All critical VT isthmuses and >80% low voltage points projected on LGE-CMR scar	Good correlation between EAM- and LGE-CMR scar and VT isthmuses and LGE-CMR scar	39
LGE-CMR	ICM	23	>3 SD above remote normal myocardium	Electrogram voltage, duration, fractionation and isolated potentials correlated with scar transmurality (p<0.0001) 41% critical VT ablation sites located in scar core. 59% located within 10 mm of scar border 61.5% critical VT isthmuses identified in regions with 76% to 100% scar transmurality	Critical VT isthmuses correlated to increased scar transmurality.	40
LGE-CMR	NICM	19	Core: ≥50% of MSI Border zone: 35% - 50% of MSI	All target sites located within 10 mm from the LGE-CMR–derived scar area. 89% of arrhythmogenic substrates anteroseptal and inferolateral Optimal cutoff values to differentiate scar from non-scar defined by MRI: Bipolar; 2.04 mV (AUC, 0.67; sensitivity, 48%; specificity, 81%) Unipolar; 9.84 mV (AUC, 0.75; sensitivity, 73%; specificity, 69%) Endocardial bipolar voltage was only affected by scar involving the endocardial 2 mm Endocardial unipolar voltage by scar involving the endocardial 4 mm	Critical VT isthmuses located within or in close proximity to LGE-CMR scar in NICM	41

LGE-CMR	ICM and NICM	44	Core: ≥50% of MSI Border zone: 35% - 50% of MSI	74-100% critical isthmus sites located within 5 mm of >75% transmural scar 67-100% critical isthmus sites located within 5 mm of the core-border zone transition	Critical VT isthmuses correlated to increased scar transmurality and core-border zone transition zones	[42]
LGE-CMR	ICM and NICM	30	Core: ≥50% of MSI Border zone: 40% of MSI	Agreement between the conducting channels on EAM and LGE-CMR 3D left ventricular reconstructions using: 2D inversion-recovery gradient- echo sequence (2D-GRE) – 61.8% 2D single-shot inversion-recovery, no phase-sensitive reconstruction (2D-SSFP) – 37.7% 3D navigator-gated inversion recovery sequence (3D-GRE) – 79.2%	3D-GRE sequence improves the delineation of LGE-CMR conducting channels	[43]
MDCT	ICM and NICM	39	DE-MDCT	Bipolar < 1.5 mV cutoff or unipolar <8 mV cutoff; good overall concordance between DE-MDCT and EAM (K = 0.536) DE-MDCT 76% sensitivity, 86% specificity, 95% negative predictive value for scar detection 84% low amplitude points identified within 10 mm of DE-MDCT segmented scar	Good correlation between DE-MDCT and EAM-defined scar in ICM and NICM	[44]
MDCT	ICM	11	Anatomic (end-systolic and end-diastolic WT) Dynamic (wall thickening, wall motion) Perfusion (hypoenhancement)	1.5 mV cutoff; anatomic and dynamic MDCT parameters prediction of EAM scar: End-systolic WT (AUC 0.83±0.05; p=0.005) End-diastolic WT (AUC 0.75±0.06; p=0.025) Wall thickening (AUC 0.79±0.06; p=0.001) Wall motion (AUC 0.68±0.06; p=0.019) 1.5 mV cutoff; correlation between EAM- and CT hypoperfusion-defined scar (r=0.77; p=0.006)	CT hypoperfusion demonstrates best correlation with EAM-defined scar	[45]
MDCT	ICM	13	WT (<5 mm)	1.5 mV cutoff; good correlation between endocardial EAM scar and MDCT regions with <5 mm WT (R=0.82; p=0.001) 1.5 mV cutoff; no significant correlation between epicardial EAM scar and MDCT regions with <5 mm WT (R=0.55; p=0.13) 100% LAVA located within 23 mm of MDCT (<5 mm) scar	Good correlation between endocardial EAM-scar and MDCT WT Poor correlation between epicardial EAM- scar and MDCT WT Large proportion of LAVA located within or in close proximity to MDCT-defined scar	[46]
MDCT	ICM, NICM, ARVC	106	WT (<5 mm) in ICM and NICM	1.5 mV cutoff; agreement between MDCT- and EAM-defined substrate higher in ICM and ARVC as compared to NICM Endocardium: ICM 66±14%; ARVC 60±16%; NICM 13±16%, P<0.0001	Good correlation between EAM-defined scar and MDCT WT in ICM and MDCT hypoattenuation in ARVC	[38]

			Hypoattenuation in ARVC	Epicardium: ICM 60±14%; ARVC 68±20%; NICM 23±21%, P<0.001 ICM: 88% LAVA located within MDCT scar NICM: 72% LAVA located within MDCT scar	Poor correlation between EAM-scar and MDCT WT in NICM A large proportion of VT substrate (LAVA) located within or in close proximity to MDCT-defined scar	
PET-CT	ICM	19	Uptake <50% of maximum	1.5 mV cutoff; agreement between PET-CT and EAM-scar; % error 18.5±7.7 0.9 mV cutoff; agreement between PET-CT and EAM-scar; % error 2.4±1.1 0.5 mV cutoff; agreement between PET-CT and EAM-scar; % error 13.5±9.6	A threshold of 0.9 mV results in the most robust correlation between EAM and PET-CT.	[47]
PET-CT	ICM	10		1.5 mV cutoff; good correlation between PET-CT and EAM-defined scar (r=0.71, p=0.076) 40% metabolic threshold correlated well with EAM scar 46% metabolic threshold correlated well with EAM scar and scar border zone	Good correlation between PET-CT and EAM-scar	[48]
PET-CT	ICM and NICM	14	Uptake <50% of maximum	50% metabolic activity threshold; 89% sensitivity, 93% specificity to predict EAM-defined scar 0.5 mV cutoff; good correlation between PET-CT and EAM-defined scar (r=0.89, p<0.05)	Good correlation between PET-CT and EAM-scar	[49]
SPECT	ICM and NICM	10		SPECT-defined scar matched in 72% of EAM-defined scar segments All successful ablation sites located within the SPECT defined scar or within 1 cm of its border	Moderate correlation between SPECT and EAM-scar	[50]

Abbreviations: 3D-GRE, three dimensional gradient recalled echo; ARVC, arrhythmogenic right ventricular cardiomyopathy; AUC, area under curve; DE-MDCT, delayed enhancement MDCT; LGE-CMR, delayed enhancement MRI; EAM, electro-anatomical map; ICM, ischaemic cardiomyopathy; LAVA, local abnormal ventricular activities; MSI, maximum signal intensity; NICM, non-ischaemic cardiomyopathy; PET-CT, positron emission tomography CT; SD, standard deviation; SI, signal intensity; VT, ventricular tachycardia; WT wall thinning

Supplemental references

1. Dawson DK, Hawlisch K, Prescott G, Roussin I, Di Pietro E, Deac M, Wong J, Frenneaux MP, Pennell DJ and Prasad SK. Prognostic role of CMR in patients presenting with ventricular arrhythmias. *JACC Cardiovasc Imaging*. 2013;6:335-44.
2. Yan AT, Shayne AJ, Brown KA, Gupta SN, Chan CW, Luu TM, Di Carli MF, Reynolds HG, Stevenson WG and Kwong RY. Characterization of the peri-infarct zone by contrast-enhanced cardiac magnetic resonance imaging is a powerful predictor of post-myocardial infarction mortality. *Circulation*. 2006;114:32-9.
3. Scott PA, Morgan JM, Carroll N, Murday DC, Roberts PR, Peebles CR, Harden SP and Curzen NP. The extent of left ventricular scar quantified by late gadolinium enhancement MRI is associated with spontaneous ventricular arrhythmias in patients with coronary artery disease and implantable cardioverter-defibrillators. *Circ Arrhythm Electrophysiol*. 2011;4:324-30.
4. Schmidt A, Azevedo CF, Cheng A, Gupta SN, Bluemke DA, Foo TK, Gerstenblith G, Weiss RG, Marban E, Tomaselli GF, Lima JA and Wu KC. Infarct tissue heterogeneity by magnetic resonance imaging identifies enhanced cardiac arrhythmia susceptibility in patients with left ventricular dysfunction. *Circulation*. 2007;115:2006-14.
5. Gulati A, Jabbour A, Ismail TF, Guha K, Khwaja J, Raza S, Morarji K, Brown TD, Ismail NA, Dweck MR, Di Pietro E, Roughton M, Wage R, Daryani Y, O'Hanlon R, Sheppard MN, Alpendurada F, Lyon AR, Cook SA, Cowie MR, Assomull RG, Pennell DJ and Prasad SK. Association of fibrosis with mortality and sudden cardiac death in patients with nonischemic dilated cardiomyopathy. *JAMA*. 2013;309:896-908.
6. Neilan TG, Coelho-Filho OR, Danik SB, Shah RV, Dodson JA, Verdini DJ, Tokuda M, Daly CA, Tedrow UB, Stevenson WG, Jerosch-Herold M, Ghoshhajra BB and Kwong RY. CMR quantification of myocardial scar provides additive prognostic information in nonischemic cardiomyopathy. *JACC Cardiovasc Imaging*. 2013;6:944-54.
7. Iles L, Pfluger H, Lefkovits L, Butler MJ, Kistler PM, Kaye DM and Taylor AJ. Myocardial fibrosis predicts appropriate device therapy in patients with implantable cardioverter-defibrillators for primary prevention of sudden cardiac death. *J Am Coll Cardiol*. 2011;57:821-8.
8. Assomull RG, Prasad SK, Lyne J, Smith G, Burman ED, Khan M, Sheppard MN, Poole-Wilson PA and Pennell DJ. Cardiovascular magnetic resonance, fibrosis, and prognosis in dilated cardiomyopathy. *J Am Coll Cardiol*. 2006;48:1977-85.
9. Bello D, Fieno DS, Kim RJ, Pereles FS, Passman R, Song G, Kadish AH and Goldberger JJ. Infarct morphology identifies patients with substrate for sustained ventricular tachycardia. *J Am Coll Cardiol*. 2005;45:1104-8.
10. Boye P, Abdel-Aty H, Zacharzowsky U, Bohl S, Schwenke C, van der Geest RJ, Dietz R, Schirdewan A and Schulz-Menger J. Prediction of life-threatening arrhythmic events in patients with chronic myocardial infarction by contrast-enhanced CMR. *JACC Cardiovasc Imaging*. 2011;4:871-9.
11. Fernandes VR, Wu KC, Rosen BD, Schmidt A, Lardo AC, Osman N, Halperin HR, Tomaselli G, Berger R, Bluemke DA, Marban E and Lima JA. Enhanced infarct border zone function and altered mechanical activation predict inducibility of monomorphic

ventricular tachycardia in patients with ischemic cardiomyopathy. *Radiology*. 2007;245:712-9.
12. Roes SD, Borleffs CJ, van der Geest RJ, Westenberg JJ, Marsan NA, Kaandorp TA, Reiber JH, Zeppenfeld K, Lamb HJ, de Roos A, Schalij MJ and Bax JJ. Infarct tissue heterogeneity assessed with contrast-enhanced MRI predicts spontaneous ventricular arrhythmia in patients with ischemic cardiomyopathy and implantable cardioverter-defibrillator. *Circ Cardiovasc Imaging*. 2009;2:183-90.
13. de Haan S, Meijers TA, Knaapen P, Beek AM, van Rossum AC and Allaart CP. Scar size and characteristics assessed by CMR predict ventricular arrhythmias in ischaemic cardiomyopathy: comparison of previously validated models. *Heart*. 2011;97:1951-6.
14. Yokokawa M, Tada H, Koyama K, Ino T, Hiramatsu S, Kaseno K, Naito S, Oshima S and Taniguchi K. The characteristics and distribution of the scar tissue predict ventricular tachycardia in patients with advanced heart failure. *Pacing Clin Electrophysiol*. 2009;32:314-22.
15. Klem I, Weinsaft JW, Bahnson TD, Hegland D, Kim HW, Hayes B, Parker MA, Judd RM and Kim RJ. Assessment of myocardial scarring improves risk stratification in patients evaluated for cardiac defibrillator implantation. *J Am Coll Cardiol*. 2012;60:408-20.
16. Wu KC, Gerstenblith G, Guallar E, Marine JE, Dalal D, Cheng A, Marban E, Lima JA, Tomaselli GF and Weiss RG. Combined cardiac magnetic resonance imaging and C-reactive protein levels identify a cohort at low risk for defibrillator firings and death. *Circ Cardiovasc Imaging*. 2012;5:178-86.
17. Piers SR, Everaerts K, van der Geest RJ, Hazebroek MR, Siebelink HM, Pison LA, Schalij MJ, Bekkers SC, Heymans S and Zeppenfeld K. Myocardial scar predicts monomorphic ventricular tachycardia but not polymorphic ventricular tachycardia or ventricular fibrillation in nonischemic dilated cardiomyopathy. *Heart Rhythm*. 2015;12:2106-14.
18. Chimura M, Kiuchi K, Okajima K, Shimane A, Sawada T, Onishi T, Yamada S, Taniguchi Y, gulati Y and Kawai H. Distribution of ventricular fibrosis associated with life threatening ventricular tachyarrhythmias in patients with nonishcemic dilated cardiomyopathy. *J Cardiovasc Electrophysiol*. 2015;26:1239-1246.
19. Lin LY, Su MY, Chen JJ, Lai LP, Hwang JJ, Tseng CD, Chen YS, Yu HY, Tseng WY and Lin JL. Conductive channels identified with contrast-enhanced MR imaging predict ventricular tachycardia in systolic heart failure. *JACC Cardiovasc Imaging*. 2013;6:1152-9.
20. Gao P, Yee R, Gula L, Krahn AD, Skanes A, Leong-Sit P, Klein GJ, Stirrat J, Fine N, Pallaveshi L, Wisenberg G, Thompson TR, Prato F, Drangova M and White JA. Prediction of arrhythmic events in ischemic and dilated cardiomyopathy patients referred for implantable cardiac defibrillator: evaluation of multiple scar quantification measures for late gadolinium enhancement magnetic resonance imaging. *Circ Cardiovasc Imaging*. 2012;5:448-56.
21. Wu KC, Weiss RG, Thiemann DR, Kitagawa K, Schmidt A, Dalal D, Lai S, Bluemke DA, Gerstenblith G, Marban E, Tomaselli GF and Lima JA. Late gadolinium

enhancement by cardiovascular magnetic resonance heralds an adverse prognosis in nonischemic cardiomyopathy. *J Am Coll Cardiol*. 2008;51:2414-21.
22. Grun S, Schumm J, Greulich S, Wagner A, Schneider S, Bruder O, Kispert EM, Hill S, Ong P, Klingel K, Kandolf R, Sechtem U and Mahrholdt H. Long-term follow-up of biopsy-proven viral myocarditis: predictors of mortality and incomplete recovery. *J Am Coll Cardiol*. 2012;59:1604-15.
23. Mehta D, Mori N, Goldbarg SH, Lubitz S, Wisnivesky JP and Teirstein A. Primary prevention of sudden cardiac death in silent cardiac sarcoidosis: role of programmed ventricular stimulation. *Circ Arrhythm Electrophysiol*. 2011;4:43-8.
24. Fluechter S, Kuschyk J, Wolpert C, Doesch C, Veltmann C, Haghi D, Schoenberg SO, Sueselbeck T, Germans T, Streitner F, Borggrefe M and Papavassiliu T. Extent of late gadolinium enhancement detected by cardiovascular magnetic resonance correlates with the inducibility of ventricular tachyarrhythmia in hypertrophic cardiomyopathy. *J Cardiovasc Magn Reson*. 2010;12:30.
25. Chan RH, Maron BJ, Olivotto I, Pencina MJ, Assenza GE, Haas T, Lesser JR, Gruner C, Crean AM, Rakowski H, Udelson JE, Rowin E, Lombardi M, Cecchi F, Tomberli B, Spirito P, Formisano F, Biagini E, Rapezzi C, De Cecco CN, Autore C, Cook EF, Hong SN, Gibson CM, Manning WJ, Appelbaum E and Maron MS. Prognostic value of quantitative contrast-enhanced cardiovascular magnetic resonance for the evaluation of sudden death risk in patients with hypertrophic cardiomyopathy. *Circulation*. 2014;130:484-95.
26. Bruder O, Wagner A, Jensen CJ, Schneider S, Ong P, Kispert EM, Nassenstein K, Schlosser T, Sabin GV, Sechtem U and Mahrholdt H. Myocardial scar visualized by cardiovascular magnetic resonance imaging predicts major adverse events in patients with hypertrophic cardiomyopathy. *J Am Coll Cardiol*. 2010;56:875-87.
27. Rubinshtein R, Glockner JF, Ommen SR, Araoz PA, Ackerman MJ, Sorajja P, Bos JM, Tajik AJ, Valeti US, Nishimura RA and Gersh BJ. Characteristics and clinical significance of late gadolinium enhancement by contrast-enhanced magnetic resonance imaging in patients with hypertrophic cardiomyopathy. *Circ Heart Fail*. 2010;3:51-8.
28. O'Hanlon R, Grasso A, Roughton M, Moon JC, Clark S, Wage R, Webb J, Kulkarni M, Dawson D, Sulaibeekh L, Chandrasekaran B, Bucciarelli-Ducci C, Pasquale F, Cowie MR, McKenna WJ, Sheppard MN, Elliott PM, Pennell DJ and Prasad SK. Prognostic significance of myocardial fibrosis in hypertrophic cardiomyopathy. *J Am Coll Cardiol*. 2010;56:867-74.
29. Codreanu A, Odille F, Aliot E, Marie PY, Magnin-Poull I, Andronache M, Mandry D, Djaballah W, Regent D, Felblinger J and de Chillou C. Electroanatomic characterization of post-infarct scars comparison with 3-dimensional myocardial scar reconstruction based on magnetic resonance imaging. *J Am Coll Cardiol*. 2008;52:839-42.
30. Desjardins B, Crawford T, Good E, Oral H, Chugh A, Pelosi F, Morady F and Bogun F. Infarct architecture and characteristics on delayed enhanced magnetic resonance imaging and electroanatomic mapping in patients with postinfarction ventricular arrhythmia. *Heart Rhythm*. 2009;6:644-51.

31. Bogun FM, Desjardins B, Good E, Gupta S, Crawford T, Oral H, Ebinger M, Pelosi F, Chugh A, Jongnarangsin K and Morady F. Delayed-enhanced magnetic resonance imaging in nonischemic cardiomyopathy: utility for identifying the ventricular arrhythmia substrate. *J Am Coll Cardiol*. 2009;53:1138-45.
32. Wijnmaalen AP, van der Geest RJ, van Huls van Taxis CF, Siebelink HM, Kroft LJ, Bax JJ, Reiber JH, Schalij MJ and Zeppenfeld K. Head-to-head comparison of contrast-enhanced magnetic resonance imaging and electroanatomical voltage mapping to assess post-infarct scar characteristics in patients with ventricular tachycardias: real-time image integration and reversed registration. *Eur Heart J*. 2011;32:104-14.
33. Dickfeld T, Tian J, Ahmad G, Jimenez A, Turgeman A, Kuk R, Peters M, Saliaris A, Saba M, Shorofsky S and Jeudy J. MRI-Guided ventricular tachycardia ablation: integration of late gadolinium-enhanced 3D scar in patients with implantable cardioverter-defibrillators. *Circ Arrhythm Electrophysiol*. 2011;4:172-84.
34. Fernandez-Armenta J, Berruezo A, Andreu D, Camara O, Silva E, Serra L, Barbarito V, Carotenutto L, Evertz R, Ortiz-Perez JT, De Caralt TM, Perea RJ, Sitges M, Mont L, Frangi A and Brugada J. Three-dimensional architecture of scar and conducting channels based on high resolution ce-CMR: insights for ventricular tachycardia ablation. *Circ Arrhythm Electrophysiol*. 2013;6:528-37.
35. Marra MP, Leoni L, Bauce B, Corbetti F, Zorzi A, Migliore F, Silvano M, Rigato I, Tona F, Tarantini G, Cacciavillani L, Basso C, Buja G, Thiene G, Iliceto S and Corrado D. Imaging study of ventricular scar in arrhythmogenic right ventricular cardiomyopathy: comparison of 3D standard electroanatomical voltage mapping and contrast-enhanced cardiac magnetic resonance. *Circ Arrhythm Electrophysiol*. 2012;5:91-100.
36. Perez-David E, Arenal A, Rubio-Guivernau JL, del Castillo R, Atea L, Arbelo E, Caballero E, Celorrio V, Datino T, Gonzalez-Torrecilla E, Atienza F, Ledesma-Carbayo MJ, Bermejo J, Medina A and Fernandez-Aviles F. Noninvasive identification of ventricular tachycardia-related conducting channels using contrast-enhanced magnetic resonance imaging in patients with chronic myocardial infarction: comparison of signal intensity scar mapping and endocardial voltage mapping. *J Am Coll Cardiol*. 2011;57:184-94.
37. Andreu D, Berruezo A, Ortiz-Perez JT, Silva E, Mont L, Borras R, de Caralt TM, Perea RJ, Fernandez-Armenta J, Zeljko H and Brugada J. Integration of 3D electroanatomic maps and magnetic resonance scar characterization into the navigation system to guide ventricular tachycardia ablation. *Circ Arrhythm Electrophysiol*. 2011;4:674-83.
38. Yamashita S, Sacher F, Mahida S, Berte B, Lim HS, Komatsu Y, Amraoui S, Denis A, Derval N, Laurent F, Sermesant M, Montaudon M, Hocini M, Haissaguerre M, Jais P and Cochet H. Image Integration to Guide Catheter Ablation in Scar-Related Ventricular Tachycardia. *J Cardiovasc Electrophysiol*. 2016;27:699-708.
39. Gupta S, Desjardins B, Baman T, Ilg K, Good E, Crawford T, Oral H, Pelosi F, Chugh A, Morady F and Bogun F. Delayed-enhanced MR scar imaging and intraprocedural registration into an electroanatomical mapping system in post-infarction patients. *JACC Cardiovasc Imaging*. 2012;5:207-10.

40. Sasaki T, Miller CF, Hansford R, Yang J, Caffo BS, Zviman MM, Henrikson CA, Marine JE, Spragg D, Cheng A, Tandri H, Sinha S, Kolandaivelu A, Zimmerman SL, Bluemke DA, Tomaselli GF, Berger RD, Calkins H, Halperin HR and Nazarian S. Myocardial structural associations with local electrograms: a study of postinfarct ventricular tachycardia pathophysiology and magnetic resonance-based noninvasive mapping. *Circ Arrhythm Electrophysiol*. 2012;5:1081-90.
41. Piers SR, Tao Q, van Huls van Taxis CF, Schalij MJ, van der Geest RJ and Zeppenfeld K. Contrast-enhanced MRI-derived scar patterns and associated ventricular tachycardias in nonischemic cardiomyopathy: implications for the ablation strategy. *Circ Arrhythm Electrophysiol*. 2013;6:875-83.
42. Piers SR, Tao Q, de Riva Silva M, Siebelink HM, Schalij MJ, van der Geest RJ and Zeppenfeld K. CMR-based identification of critical isthmus sites of ischemic and nonischemic ventricular tachycardia. *JACC Cardiovasc Imaging*. 2014;7:774-84.
43. Andreu D, Ortiz-Perez JT, Fernandez-Armenta J, Guiu E, Acosta J, Prat-Gonzalez S, De Caralt TM, Perea RJ, Garrido C, Mont L, Brugada J and Berruezo A. 3D delayed-enhanced magnetic resonance sequences improve conducting channel delineation prior to ventricular tachycardia ablation. *Europace*. 2015;17:938-45.
44. Esposito A, Palmisano A, Antunes S, Maccabelli G, Colantoni C, Rancoita PM, Baratto F, Di Serio C, Rizzo G, De Cobelli F, Della Bella P and Del Maschio A. Cardiac CT With Delayed Enhancement in the Characterization of Ventricular Tachycardia Structural Substrate: Relationship Between CT-Segmented Scar and Electro-Anatomic Mapping. *JACC Cardiovasc Imaging*. 2016;9:822-32.
45. Tian J, Jeudy J, Smith MF, Jimenez A, Yin X, Bruce PA, Lei P, Turgeman A, Abbo A, Shekhar R, Saba M, Shorofsky S and Dickfeld T. Three-dimensional contrast-enhanced multidetector CT for anatomic, dynamic, and perfusion characterization of abnormal myocardium to guide ventricular tachycardia ablations. *Circ Arrhythm Electrophysiol*. 2010;3:496-504.
46. Komatsu Y, Cochet H, Jadidi A, Sacher F, Shah A, Derval N, Scherr D, Pascale P, Roten L, Denis A, Ramoul K, Miyazaki S, Daly M, Riffaud M, Sermesant M, Relan J, Ayache N, Kim S, Montaudon M, Laurent F, Hocini M, Haissaguerre M and Jais P. Regional myocardial wall thinning at multidetector computed tomography correlates to arrhythmogenic substrate in postinfarction ventricular tachycardia: assessment of structural and electrical substrate. *Circ Arrhythm Electrophysiol*. 2013;6:342-50.
47. Fahmy TS, Wazni OM, Jaber WA, Walimbe V, Di Biase L, Elayi CS, DiFilippo FP, Young RB, Patel D, Riedlbauchova L, Corrado A, Burkhardt JD, Schweikert RA, Arruda M and Natale A. Integration of positron emission tomography/computed tomography with electroanatomical mapping: a novel approach for ablation of scar-related ventricular tachycardia. *Heart Rhythm*. 2008;5:1538-45.
48. Tian J, Smith MF, Chinnadurai P, Dilsizian V, Turgeman A, Abbo A, Gajera K, Xu C, Plotnick D, Peters R, Saba M, Shorofsky S and Dickfeld T. Clinical application of PET/CT fusion imaging for three-dimensional myocardial scar and left ventricular anatomy during ventricular tachycardia ablation. *J Cardiovasc Electrophysiol*. 2009;20:567-604.

49. Dickfeld T, Lei P, Dilsizian V, Jeudy J, Dong J, Voudouris A, Peters R, Saba M, Shekhar R and Shorofsky S. Integration of three-dimensional scar maps for ventricular tachycardia ablation with positron emission tomography-computed tomography. *JACC Cardiovasc Imaging*. 2008;1:73-82.
50. Tian J, Smith MF, Ahmad G, Dilsizian V, Jimenez A and Dickfeld T. Integration of 3-dimensional scar models from SPECT to guide ventricular tachycardia ablation. *J Nucl Med*. 2012;53:894-901.

Supplemental video legends

Supplemental movie 1: Diagnostic coronary angiogram in a patient undergoing epicardial VT ablation. A cine fluoroscopic image demonstrates contact between the tip of the ablation catheter and a marginal branch of the circumflex coronary artery.

Supplemental movie 2: Example of combining intra-cardiac echocardiography and CT to assist catheter navigation in a case with papillary muscle PVC. CT-derived anatomy of the cardiac chambers (*purple surface*) and papillary muscles (*blue surface*) is integrated in the CARTO system. Intra-cardiac echocardiography provides real-time assessment of catheter tip motion with respect to postero-medial papillary muscle.

Supplemental movie 3: **Example of intra-cardiac echocardiography assisting catheter navigation in a case with papillary muscle PVC**. Intra-cardiac echocardiography provides real-time assessment of catheter tip motion with respect to postero-medial papillary muscle.

Supplemental movies 4 and 5: Example of ECGI mapping to non-invasively assess VT mechanism in a case of non-ischemic dilated cardiomyopathy. Movie 4 illustrates VT activation as assessed by ECGI using a multi-electrode system. Movie 5 illustrates VT activation as assessed contact mapping in the same patient.

Supplemental movie 6: Example of image-based biophysical modelling to predict VT mechanism in a case of ischemic cardiomyopathy. CT-based data is used to personalize a 3D computationally-derived model (Eikonal model) of cardiac electrophysiology, using regional wall thickness to estimate conduction properties within the infarct. The movie illustrates activation sequences obtained from contact mapping using the Rhythmia system (*left*) and corresponding simulated activation sequences (*center and right*).

Supplemental movie 7: Example of prediction of a ventricular tachycardia circuit from MDCT imaging in a case of ischemic cardiomyopathy. The *left* image demonstrates contrast-enhanced CT delineation of myocardial scar (identified as areas of wall thinning <5 mm). Wall thickness mapping shows an anatomical channel of relatively preserved thickness between 2 areas of severe thinning on the anterior left ventricle. The movie (*right*) demonstrates the corresponding activation pattern during VT (high-density endocardial activation map obtained using the Rhythmia system). Activation mapping demonstrates co-localization between the imaging-defined anatomical channel and the critical VT isthmus.